JGR Space Physics

RESEARCH ARTICLE
10.1029/2023JA031477

Daytime Medium Scale Traveling Ionospheric Disturbances (MSTIDS) Over the Andes Mountains at Equatorial and Low Magnetic Latitudes

C. A. O. B. Figueiredo[1], C. M. Wrasse[1], S. Vadas[2], H. Takahashi[1], Y. Otsuka[3], P. K. Nyassor[1], K. Shiokawa[3], I. Paulino[4], and D. Barros[1]

[1]Space Weather Division, National Institute for Space Research—INPE, São Paulo, Brazil, [2]Northwest Research Associates, Boulder, CO, USA, [3]Institute for Space-Earth Environmental Research, Nagoya University, Nagoya, Japan, [4]Unidade acadêmica de física, Universidade Federal de Campina Grande, Campina Grande, Brazil

Key Points:

- Quiet-time daytime MSTIDs were observed at equatorial and low-geomagnetic latitudes over the Chilean and Argentinian Andes Mountains
- MSTIDs observed during summer at equatorial latitudes are most likely generated by higher-order gravity waves from the Amazon region
- Equatorial and low-geomagnetic latitude wintertime MSTIDs over the Andes may be secondary or higher-order gravity waves

Correspondence to:
C. A. O. B. Figueiredo,
anagetinga@gmail.com;
cosme.figueiredo@inpe.br

Citation:
Figueiredo, C. A. O. B., Wrasse, C. M., Vadas, S., Takahashi, H., Otsuka, Y., Nyassor, P. K., et al. (2023). Daytime medium scale traveling ionospheric disturbances (MSTIDS) over the Andes Mountains at equatorial and low magnetic latitudes. *Journal of Geophysical Research: Space Physics*, *128*, e2023JA031477. https://doi.org/10.1029/2023JA031477

Received 10 MAR 2023
Accepted 6 OCT 2023

Abstract We analyze daytime quiet-time MSTIDs between 2013 and 2015 at the geomagnetic equatorial and low latitude regions of the Chilean and Argentinian Andes using keograms of detrended total electron content (dTEC). The MSTIDs had a higher occurrence rate at geomagnetic equatorial latitudes in the June solstice (winter) and spring (SON). The propagation directions changed with the season: summer (DJF) [southeast, south, southwest, and west], winter (JJA) [north and northeast], and equinoxes [north, northeast, south, southwest, and west]. In addition, the MSTIDs at low latitudes observed between 8:00 and 12:00 UT occur more often during the December solstice and propagate northwestward and northeastward. After 12:00 UT, they are mostly observed in the equinoxes and June solstice. Their predominant propagation directions depend on the season: summer (all directions with a preference for northeastward), autumn (MAM) [north and northeast], winter (north and northeast), and spring (north, northeast, and southwest). The MSTID propagation direction at different latitudes was explained by the location of the possible sources. Besides, we calculated MSTIDs parameters at geomagnetic low latitudes over the Andes Mountains and compared them with those estimated at the geomagnetic equatorial latitudes. We found that the former is smaller on average than the latter. Also, our observations validate recent model results obtained during geomagnetically quiet-time as well as daytime MSTIDs during winter over the south of South America. These results suggest that secondary or high-order gravity waves (GWs) from orographic forcing are the most likely source of these MSTIDs.

1. Introduction

Upward-propagating atmospheric gravity waves are very important because they transfer momentum and energy from one region to the other (Alexander & Fritts, 2003). When gravity waves interact with the ionospheric plasma via neutral-ion collisions, they create oscillations in the ionosphere called traveling ionospheric disturbances (TIDs). TIDs are disturbances in the plasma with wavelengths of hundreds to thousands of kilometers and velocities of hundreds of meters per second (Hunsucker, 1982). Theoretically, this phenomenon was first investigated in the 1960s by the pioneering work of Hines (1960), although the first observation of the wavelike disturbances was in the 1940s (Munro, 1948). In the last 10 years, dozens of theoretical and observational studies in different geographic regions have been carried out using diverse instruments, such as ionosondes (e.g., Amorim et al., 2011; Sherstyukov et al., 2018), satellites (e.g., Bolmgren et al., 2020), incoherent scatter radars (e.g., Negale et al., 2018; Nicolls et al., 2010, 2014; Vadas & Nicolls, 2009), and all-sky airglow imagers (e.g., Figueiredo et al., 2018b; Martinis et al., 2019; Paulino et al., 2016; Smith et al., 2013; Terra et al., 2020), total electron content (e.g., Azeem et al., 2015, 2017; Chen et al., 2019; Essien et al., 2021, 2022; Figueiredo et al., 2018a; Sivakandan et al., 2021), and Doppler radar sounder (Crowley & Rodrigues, 2012; Vadas & Crowley, 2010).

Daytime MSTIDs are mainly induced by gravity waves "from below" via neutral-ion collisions. The daytime MSTIDs are generated by gravity waves originating in different regions of the atmosphere via neutral-ion collisions (e.g., Azeem et al., 2015; Figueiredo et al., 2018b; Nishioka et al., 2013; Paulino et al., 2016). For example, Vadas and Crowley (2010) observed northward propagating TIDs over Wallops Island and concluded that these TIDs were induced by secondary GWs from the dissipation of primary GWs excited by tropical storm Noel. It is known that the propagation direction of these waves is different for each location due to the source and/or wind filtering (Figueiredo et al., 2018a).

The sources of gravity waves (which induce the MSTIDs) have been of interest for many decades because they provide information about the characteristics of the observed MSTIDs. The primary sources are deep convective storms (Alexander & Pfister, 1995; Azeem-Barlage, 2017; Azeem et al., 2015; Heale et al., 2019; Lane et al., 2001; Vadas & Azeem, 2020; Vadas & Crowley, 2010; Vadas, Liu, & Lieberman, 2014; Xu et al., 2019), ocean waves (Vadas et al., 2015; Zabotin et al., 2016), tsunamis (Azeem et al., 2017; Hickey et al., 2009; Makela et al., 2011; Occhipinti et al., 2006), meteor ablation (Vadas, Suzuki, et al., 2014), earthquakes (Galvan et al., 2012), tornadoes (Nishioka et al., 2013), auroral heating (Figueiredo et al., 2017), orography (Alexander et al., 2015; De la Torre et al., 2014; Smith et al., 2013; Vadas & Nicolls, 2009; Vadas et al., 2019), among others.

The longest mountain range in the world is in South America: the Andes Mountains. Mountain waves are generated when the wind flows over a mountain (Alexander & Fritts, 2003; Holton, 1992). During the winter, these waves propagate upward into the stratosphere and possibly into the mesosphere before breaking and/or reaching critical levels (Fritts et al., 2021; Heale et al., 2020; Lund et al., 2020; Sato et al., 2012). Using a high-resolution general circulation model, Becker and Vadas (2018) and Vadas et al. (2018) showed that secondary gravity waves are generated by the local body forces (i.e., horizontal accelerations) created from the deposition of momentum that occurs from the breaking of mountain waves in the stratosphere. They found that these secondary GWs propagate upward to the mesosphere and lower thermosphere (MLT). They also found that where these secondary gravity waves break or dissipate from molecular viscosity, local body forces are created, which generate upward- and downward-propagating tertiary GWs. Vadas and Becker (2019), Vadas et al. (2019), and Becker and Vadas (2020) showed through numerical simulation and observations that most of the wintertime (JJA) gravity waves observed above 130 km altitude are likely tertiary gravity waves created by the dissipation of secondary GWs from mountain wave breaking. Indeed, Becker and Vadas (2020) reproduced, for the first time, the wintertime GW hotspot seen in the GOCE and CHAMP satellites over the Southern Andes at $z \sim 250$–400 km.

Many studies on MSTIDs are conducted at middle and high geomagnetic latitudes around the world (e.g., Ding et al., 2011; Ishida et al., 2008; Kotake et al., 2007; Negale et al., 2018; Otsuka et al., 2011, 2013). On the other hand, only a few studies have been conducted at equatorial and low magnetic latitudes over the Andes Mountains, and those published studies are during the nighttime (e.g., Duly et al., 2013; Martinis et al., 2006). Therefore, the goal of the present study is to fill in this gap by characterizing the wavelength, horizontal phase speed, period, propagation direction, and seasonality of the daytime MSTIDs at equatorial and low magnetic latitudes observed in the vicinity of the Andes Mountains. We will also discuss whether the orography of the Andes can produce gravity waves that can propagate vertically and disturb the ionospheric plasma through multi-step vertical coupling (e.g., Becker & Vadas, 2020; Vadas & Becker, 2019; Vadas et al., 2019). Additionally, the characteristics of the MSTIDs observed between the East and West coasts of South America will be compared. This study also would help models to improve their predictive power in forcasting MSTIDs induced by gravity waves from the lower atmosphere via detailed comparison with these observations.

2. Methodology

Figure 1 shows approximately 80 GNSS receivers located around the Andes Mountains. The slant TEC (STEC) can be calculated using the phase delay for each wave frequency L1 and L2 between the GPS satellite and ground receiver every 30 s, which can be derived using Equation 1 (Mannucci et al., 1998):

$$\mathrm{STEC} = \frac{1}{40.3}\frac{f_1^2 f_2^2}{f_1^2 - f_2^2}[(L_1 - L_2) - (\lambda_1 N_1 - \lambda_2 N_2) + b_r + b_s], \quad (1)$$

where L_1 and L_2 are the phase delay of the signal converted to distance unit; $\lambda_1 N_1$ and $\lambda_2 N_2$ are the integer phase ambiguities; and b_r and b_s are instrumental biases of the receiver and satellite, respectively. The goal of this analysis is to obtain the vertical TEC (VTEC) perturbations and then to study MSTIDs following the same procedure as Kotake et al. (2007), Otsuka et al. (2011, 2013), and Tsugawa et al. (2007). The STEC was converted from slant to vertical using a single-layer model at 300 km altitude. Furthermore, the vertical TEC data with elevation angles less than 30° were excluded to reduce the problem of cycle slips. Then, the detrended TEC (dTEC) is calculated by subtracting a 1 hr running average (centered at ±30 min) from the original VTEC time series (Figueiredo et al., 2017; Tsugawa et al., 2007). We chose a 1 hr running average to extract the MSTIDs because the time series of each pseudo-random number (PRN) are typically only 2–3 hr long. This technique can only be used to observe MSTIDs and LSTIDs with periods less than 1 hr (e.g., Figueiredo et al., 2017; Tsugawa et al., 2007). Although

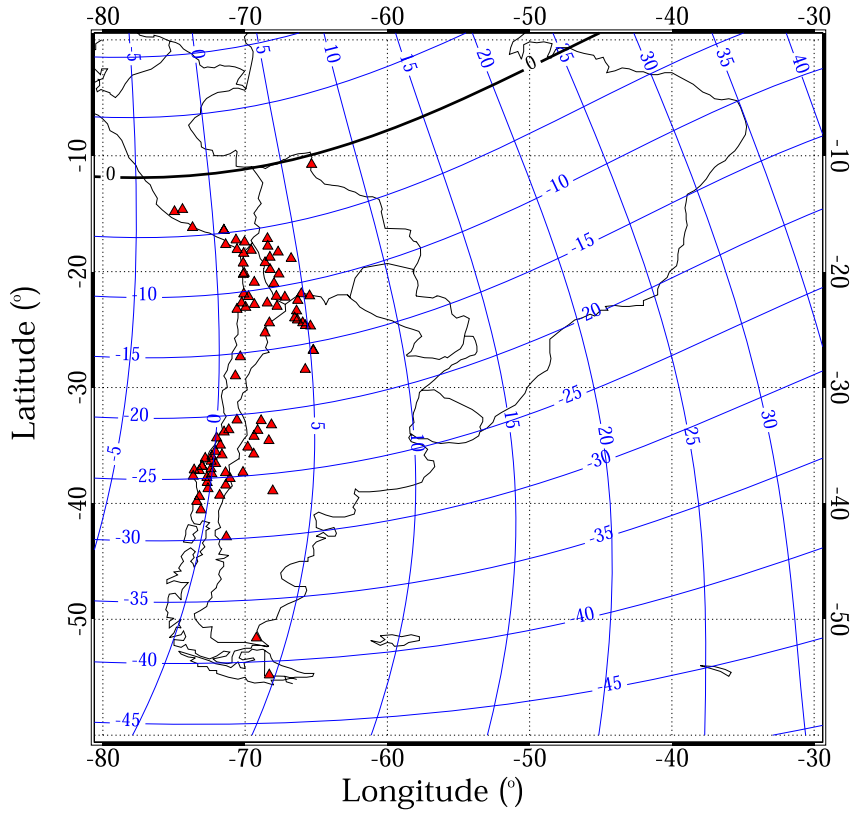

Figure 1. The GNSS receiver locations (red triangles) over the Andes from 2013 to 2015. The black line represents the magnetic equator (at 300 km altitude); the blue lines represent the magnetic field lines and the quasi-dipole latitude.

this includes all MSTIDs, it only comprises the higher-frequency LSTIDs with periods <1 hr, since the periods of LSTIDs, in general, are 30 min to several hours (Hocke & Schlegel, 1996; Hunsucker, 1982). Since this paper focuses only on analyzing MSTIDs, this method suits our objective.

dTEC keograms (latitude vs. time and longitude vs. time plots) were made using cuts at six latitudes (20°S, 22.5°S, 25°S, 32.5°S, 35°S, and 37.5°S) and four longitudes (68.5°W, 70°W, 71.5°W, and 73°W); this resulted in the generation of twenty-four keograms per day. These keograms have a time resolution of 1 min and a spatial resolution of 0.2° × 0.2° in longitude and latitude. To minimize the lack of data in dTEC keograms, the grid was smoothed by 1° × 1° in latitude and longitude, the same methodology adopted by Figueiredo et al. (2017, 2018a).

The goal was to study the MSTIDs at different latitudes, that is, at equatorial geomagnetic latitudes (between low geographic 15°S and 30°S) and low geomagnetic latitudes (between middle geographic 30°S and 45°S) in the Chilean and Argentinian Andes. In addition, the TIDs parameters were calculated using the geographical coordinates because the geomagnetic declination in South America is the largest. Such a large difference in latitude makes it challenging to calculate the characteristics and compare TIDs in different regions using geomagnetic coordinates. Also, it is important to mention that the geographic low and middle latitudes over the South American continent correspond to the geomagnetic equatorial to low latitudes, respectively (see Figure 1). Those regions are located inside the crest of the Equatorial Ionization Anomaly. Therefore, the high electron density in this region could affect the MSTIDs propagation. Details are given in the discussion section.

A total of 26,280 keograms were made in order to detect, characterize, and analyze the observed MSTIDs between 2013 and 2015. For each day, we made 24 keograms for the latitude and longitude cuts listed above. We identified an MSTID event by manually visually inspecting all 24 cuts. For each region, time interval, and event, we chose only the keogram that best shows the structure of the MSTID. We used the criteria established by Kotake et al. (2007), Otsuka et al. (2011, 2013), and Figueiredo et al. (2018a):

1. The amplitude of the oscillation of the dTEC must exceed 0.2 TECU; although the dTEC data contains MSTIDs with amplitudes of 0.1–0.2 TECU (and smaller than 0.1 TECU), it is often quite noisy. This may

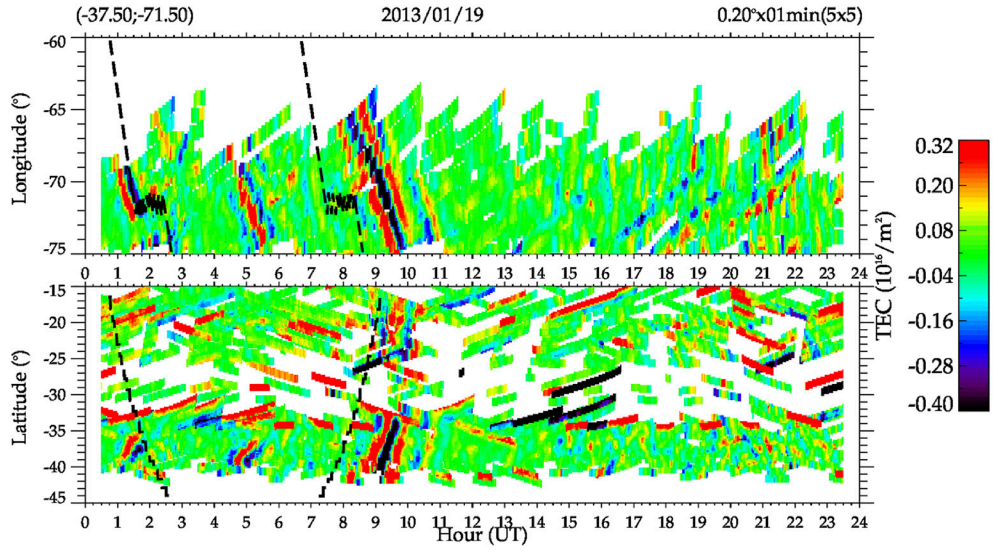

Figure 2. Keograms of the zonal (upper panel) at 71.5°W and meridional (lower panel) at 37.5°S component on 19 January 2013. The dashed black lines represent the dusk and dawn terminators at 300 km height. The break in the solar terminator dashed line is due to the low spatial and temporal resolution during the longitude variation.

be in part due to the fact that we did not remove acoustic waves from the data here. Because we only want to analyze clearly visible MSTIDs, we have chosen our threshold cutoff to be dTEC > 0.2 TECU for the analysis we perform on the MSTIDs here;

2. The horizontal wavelength is shorter than 1,500 km;
3. The period is less than 60 min;
4. The oscillation must have more than two wavefronts and must be propagating on the maps or in the keograms. We assume that the propagation direction is perpendicular to the wavefront of the MSTIDs, which is a characteristic of gravity waves (Hines, 1960). We have also selected wavefronts greater than 3° in latitude and longitude in the keograms.

In order to extract the parameters of the MSTIDs, we used the discrete Fourier transform (DFT) in both zonal and meridional keograms employing the methodology of Figueiredo et al. (2018a). First, we calculate the period (τ) in both the zonal and meridional keograms using DFT. Here, we select the same area (in km) in the zonal and meridional keograms over the same time interval to perform the DFT. Next, the DFT cross-spectrum, from which the amplitude (A) and phase ($\Delta\psi$) are estimated. Then, we calculate the horizontal wavelength ($\lambda_H = \lambda_{NS}\lambda_{EW}/\sqrt{\lambda_{NS}^2 + \lambda_{EW}^2}$); where $\lambda_{NS},\lambda_{EW} = \Delta d/(\Delta\psi/360^\circ)$, Δd is the distance between the time series; horizontal phase speed ($C_H = \lambda_H/\tau$), and propagation direction ($\theta = \cos^{-1}(\lambda_H/\lambda_{NS})$) of the MSTID using both the zonal and meridional keograms.

As an example, Figure 2 shows the keograms in the zonal and meridional directions on 19 January 2013. The horizontal axis indicates the time with a temporal resolution of 1 minute, and the vertical axis represents distances in degrees. These keograms were generated for the latitude cut at 37.5°S for the zonal keogram (upper panel) and the longitude cut at 71.5°W for the meridional keogram (lower panel). The black dashed lines indicate the times and locations where the solar terminator at 300 km altitude crosses the region of study. In Figure 2, we observe three MSTIDs. The first occurs at night, between 04:00 and 06:00 UT, and propagates northwestward. It has a λ_H of 366 ± 71 km, C_H of 104 ± 21 m/s, and a τ of 59 ± 3 min. The second MSTID occurs before dusk solar terminator between 01:00 and 02:00 UT and is observed propagating northwestward with a λ_H of 389 ± 81 km, C_H of 147 ± 32 m/s, and τ of 44 ± 2 min. Finally, just after the dawn solar terminator crossed the keogram cut region (08:00-10:00 UT), a daytime MSTID is observed propagating in the same direction as the solar terminator. It has a λ_H of 468 ± 178 km, a C_H of 138 ± 53 m/s, and a τ of 56 ± 3 min. To calculate the uncertain values in the MSTID parameters, we assume an uncertainty of 5% of the period calculated by DFT based on the significance level estimated at 95%. The significance level is calculated using white noise by Torrence and Compo (1998) method. Next, we estimate the wavelength, phase speed, and propagation direction uncertainties using the general uncertainty propagation equation from Bevington and Robinson (2003) [Equation 3.14, pg. 41].

3. Statistical Results

We analyzed dTEC data obtained in the region of the Chilean Andes Mountains, including a part of Argentina and Peru, from January 2013 to December 2015, and we found 2173 MSTIDs. Each year was divided into four seasons: summer (December–February), autumn (March–May), winter (June–August), and spring (September–November). In addition, the results are divided into two groups, geomagnetic equatorial (geographic low (15–30°)) and geomagnetic low (geographic middle (30–45°)).

3.1. Geomagnetic Equatorial Latitude Daytime MSTIDs

Between 2013 and 2015, 1120 MSTID events were observed at geomagnetic equatorial latitudes. However, here we only consider daytime and quiet-time MSTID events with Kp $\leq$ 3, which results in a total of 946 MSTID events. Figures 3a–3c show plots of the general characteristics of the MSTIDs: (a) horizontal wavelength, (b) horizontal phase speed, and (c) observed period as a function of the number of MSTID events. To better understand the relationship between the MSTID parameters, Figures 3d–3f show contour plots of the number of MSTID events: (d) MSTIDs period versus horizontal wavelength, (e) horizontal phase speed versus horizontal wavelength, and (f) period versus horizontal phase speed. The color bar indicates the number of MSTID events. Figures 3d and 3e show that the shorter period MSTIDs have smaller horizontal wavelengths and slower horizontal phase speed have smaller horizontal wavelengths. Also, from Figure 3f, the relationship between period and horizontal phase speed does show this linear correspondence. Therefore, these results corroborate the results found in Figure 12 of Vadas and Crowley (2010). On the other hand, Rows 3–6 show the MSTIDs characteristics results for each season.

Figure 4 shows the quiet-time daytime MSTID monthly occurrence rate as a function of time. The occurrence rate is defined as a fraction of the number of days that MSTIDs were observed divided by the total number of days in each month, the same method used by Figueiredo et al. (2018a) and Otsuka et al. (2013). For example, if an MSTID was observed for 6 hr, from 12 to 18 UT, we divided it into 6 bins of an hour each because we observed it for a total of 6 hr. Also, the daytime MSTIDs are defined when the observation start and end time is between 8 and 24 UT. In this way, we discard MSTIDs when there is a transition between day to night and vice-versa. Figure 4 shows that the highest occurrence of MSTIDs is in the winter months between 14:00 and 22:00 UT and during the equinoxes between 18:00 and 24:00 UT (UT = LT + 4 hr).

Figure 5 shows the propagation directions of daytime MSTIDs at geomagnetic equatorial latitudes in the Andean sector. During the summer solstice (Figure 5a), the MSTIDs propagate to the southeast, south, southwest, and west. On the other hand, during the winter solstice (Figure 5c), the MSTIDs propagate to the northwest, north, and northeast. Furthermore, during the equinoxes (Figures 5b and 5d), the MSTIDs propagate predominately to the north, south, southwest, and west.

Figure 6 shows the propagation directions of daytime MSTIDs in the Andes geomagnetic equatorial latitudes as a function of the time. During the winter (Figure 6c), between 12 and 24 UT, there is no change in the propagation direction over time. However, during the equinoxes (Figures 6b and 6d), the propagation directions changed with the local time. MSTIDs propagate equatorward between 14 and 21 UT, then, near dusk, between 20 and 24 UT, they propagate southeast, south, southwest, and west. During summer solstice (Figure 6a), the MSTIDs between 12 and 23 UT propagate southeast and south. Moreover, after 17 UT, they propagate southwest.

3.2. Geomagnetic Low Latitude Daytime MSTIDs

At geomagnetic low latitude, we observed 1053 MSTID events from 2013 to 2015. Here, we only analyze daytime and quiet-time events with Kp $\leq$ 3, for a total of 726 MSTID events. Some of the MSTIDs observed at geomagnetic low latitudes were also observed at geomagnetic equatorial latitudes. Figures 7a–7c show plots of the general characteristics of the MSTIDs: (a) horizontal wavelength, (b) horizontal phase speed, and (c) observed period as a function of the number of MSTID events. Figures 7d–7f show contour plots of the number of MSTID events: (d) MSTIDs period versus horizontal wavelength, (e) horizontal phase speed versus horizontal wavelength, and (f) period versus horizontal phase speed. The color bar indicates the number of MSTID events. Rows 3–6 show the corresponding results for each season, as labeled. For all the seasons, the MSTIDs have average values of the horizontal wavelength, horizontal phase speed, and period of 436 $\pm$ 139 km, 241 $\pm$ 65 m/s, and 31 $\pm$ 6 min,

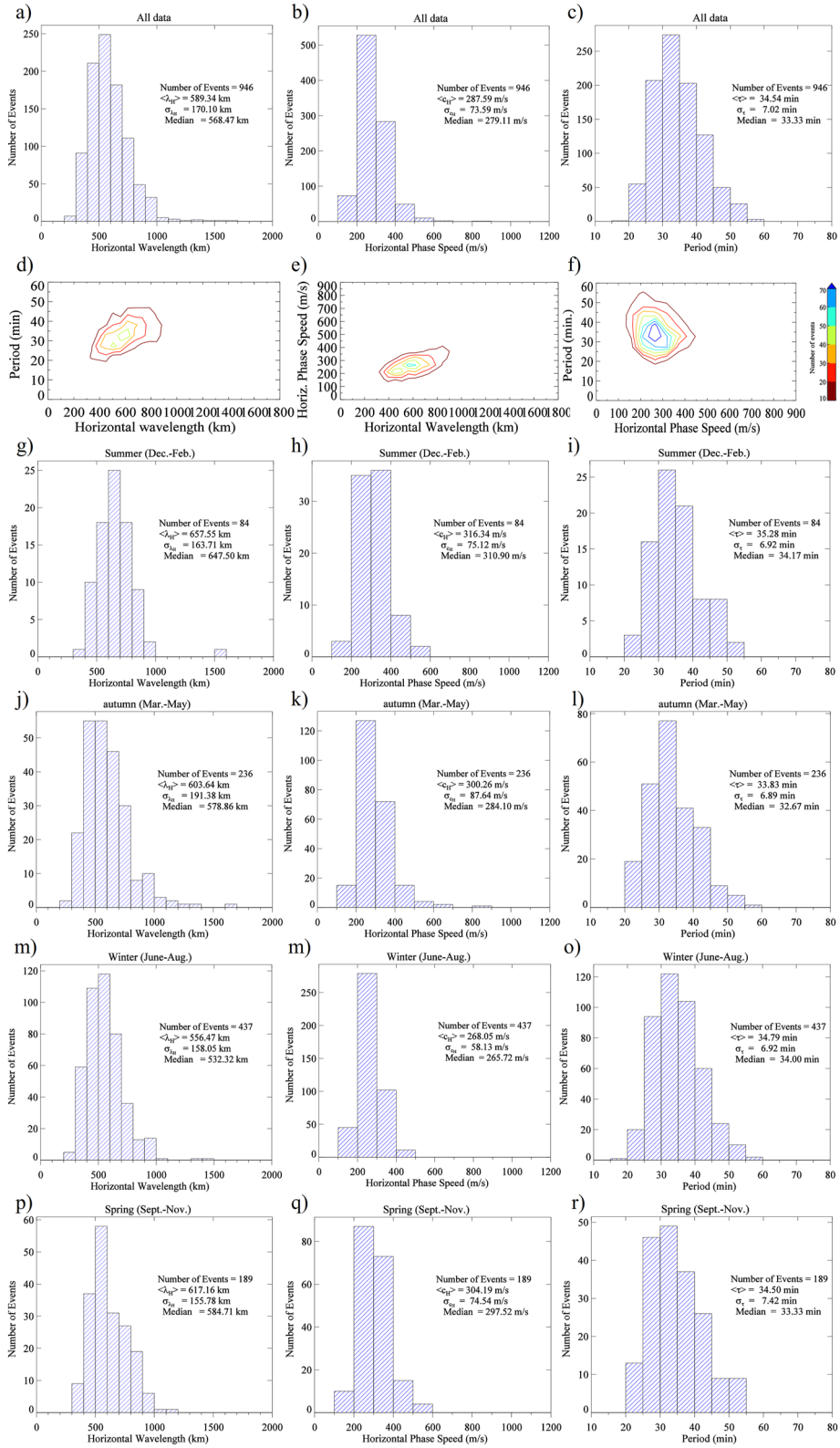

Figure 3. Characteristics of the quiet-time daytime MSTIDs observed at geomagnetic equatorial latitudes in the Andean sector from 2013 to 2015. (a–c): plots as a function of the number of MSTID events: (a) horizontal wavelength, (b) horizontal phase speed, (c) observed period. (d–f): contour plots showing the number of MSTID events: (d) observed period versus horizontal wavelength, (e) horizontal phase speed versus horizontal wavelength, and (f) observed period versus horizontal phase speed. The color bar indicates the number of MSTIDs in (d-f). Rows 3–6 show the corresponding results for each season, as labeled.

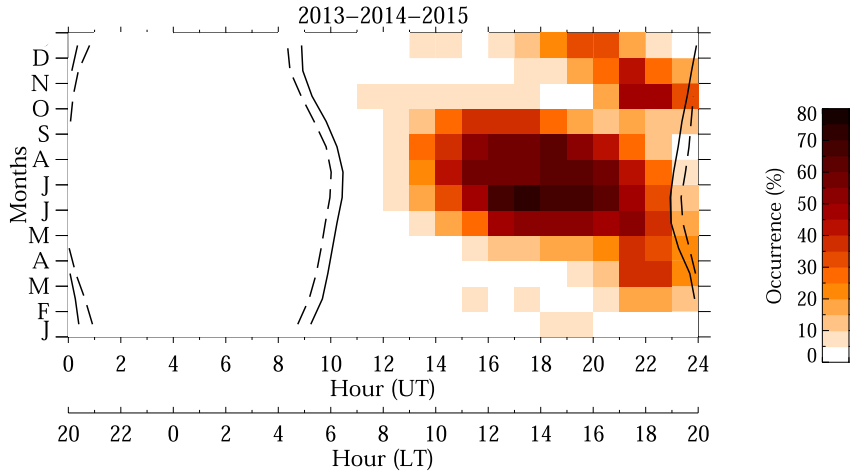

Figure 4. Quiet-time daytime MSTID occurrence rate as a function of time in the Andean sector at geomagnetic equatorial latitudes. Data from January 2013 to December 2015. The black dashed-dot-dot-dot and dashed lines show the solar terminator for heights of 110 and 300 km, respectively.

respectively. The average values of the horizontal wavelength and horizontal phase speed at geomagnetic low latitude (436 ± 139 km and 241 ± 65 m/s) are smaller than the horizontal wavelength and horizontal phase speed observed (589 ± 170 km and 288 ± 74 m/s) at geomagnetic equatorial latitude (Figures 3a and 3b). We test the null hypothesis that there is no difference between the geomagnetic equatorial and low latitude daytime MSTIDs

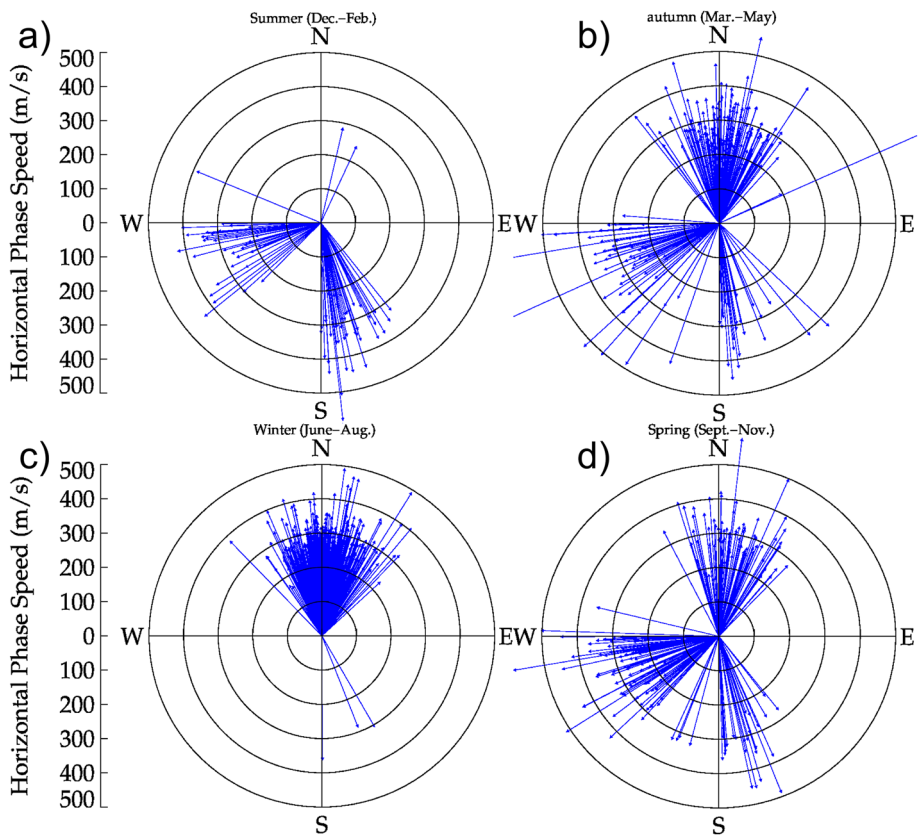

Figure 5. The propagation directions of quiet-time daytime MSTIDs at geomagnetic equatorial latitudes during (a) summer (Dec.–Feb.), (b) autumn (March–May), (c) winter (June–August), and (d) spring (September–November). Each circular line indicates a constant horizontal phase speed.

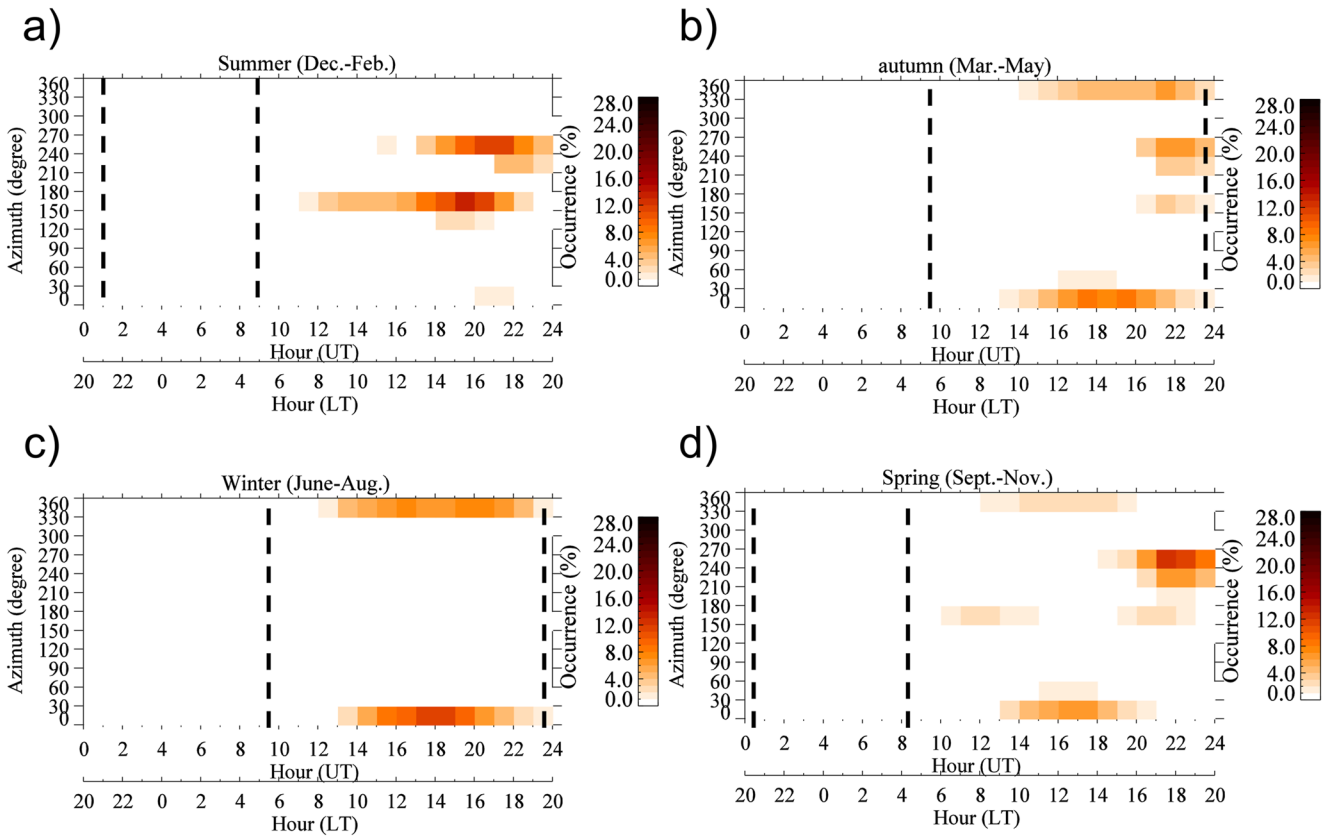

Figure 6. Local time dependency of the propagation direction of quiet-time geographic low latitudes MSTIDs for (a) summer, (b) autumn, (c) winter, and (d) spring. The black dashed lines show the solar terminator.

characteristics versus whether there is a statistical difference between geomagnetic equatorial and low latitude daytime MSTIDs characteristics. Similarly, the non-parametric statistical test known as Wilcoxon-Mann-Whitney (M. Neuhäuser, 2011) was applied. The interpretations of the statistical test showed that the *p*-value for this test (2.2e−16), which is small (<0.05), that is, rejecting the null hypothesis, indicating that there is statistically significant evidence that geomagnetic equatorial and low latitude daytime MSTIDs characteristics are different. Also, Figures 7d and 7e show that the shorter period MSTIDs have smaller horizontal wavelengths and slower horizontal phase speeds. On the other hand, in Figure 3f, the relationship between period and horizontal phase speed does not show this linear correspondence. Therefore, the shorter period MSTIDs have smaller horizontal wavelengths and shorter horizontal phase speed have smaller horizontal wavelength corroborating the results found in Figure 12 of Vadas and Crowley (2010) and similar results to the geomagnetic equatorial latitude MSTIDs (Figures 3d and 3e).

Figure 8 shows the monthly occurrence rate of geomagnetic low latitude daytime MSTIDs. We note that the highest occurrence of daytime MSTIDs occurs during the winter and equinoxes months between 14:00 and 21:00 UT (LT = UT – 4). As shown above in Figures 7j–7r, during the winter and equinox, daytime MSTIDs have horizontal wavelengths between 200 and 1,000 km, periods ranging from 15 to 60 min, and horizontal phase speeds of 100–600 m/s. Furthermore, MSTIDs between 08:00 and 12:00 UT have horizontal wavelengths of 242–914 km, 27–60 min periods, and horizontal phase speeds of 108–362 m/s (not shown); these MSTIDs may be related to the passage of the solar terminator, as we discuss further in Section 4.2.

Figure 9 shows the propagation directions of geomagnetic low) latitude quiet-time daytime (blue vectors) MSTIDs. During the summer solstice (i.e., Figure 9a), we observe that MSTIDs propagate in almost all directions with a preference in the northeastward direction. During equinox months (Figures 9b and 9d), they propagate to the north, northeast, and southwest but the majority propagate north-northeast. On the other hand, during the winter solstice (Figure 9c), the MSTIDs propagate to the northwest, north, and northeast. It is important to note

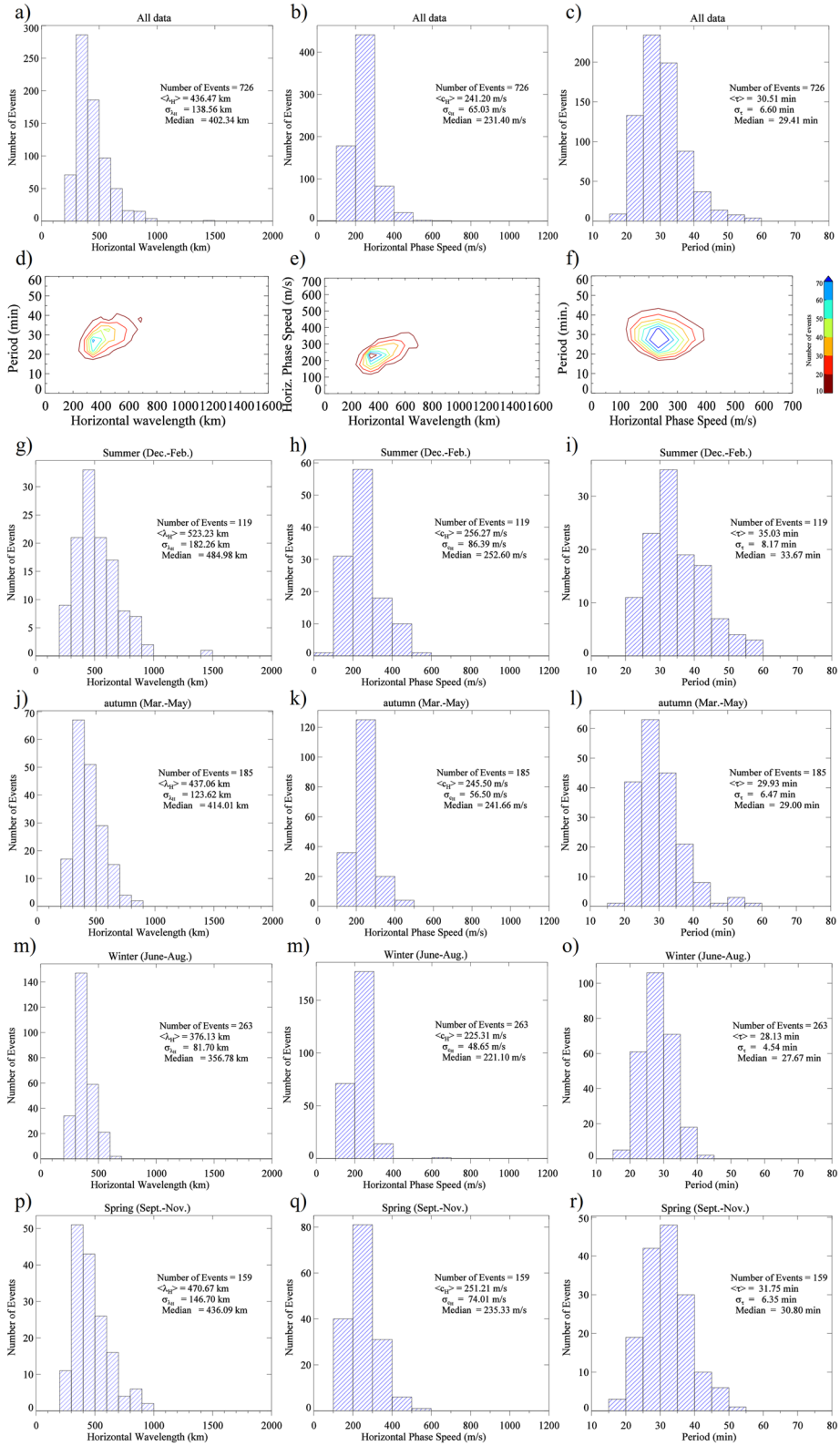

Figure 7. Characteristics of the quiet-time daytime MSTIDs observed at geomagnetic low latitudes in the Andean sector between 2013 and 2015. (a–c): 1D plots as a function of the number of MSTID events: (a) horizontal wavelength, (b) phase speed, (c) observed period. (d–f): 2D contour plots showing the number of MSTID events: (d) observed period versus horizontal wavelength, (e) horizontal phase speed versus horizontal wavelength, and (f) observed period versus horizontal phase speed. The color bar indicates the number of MSTIDs in (d–f). Rows 3–6 show the corresponding results for each season, as labeled.

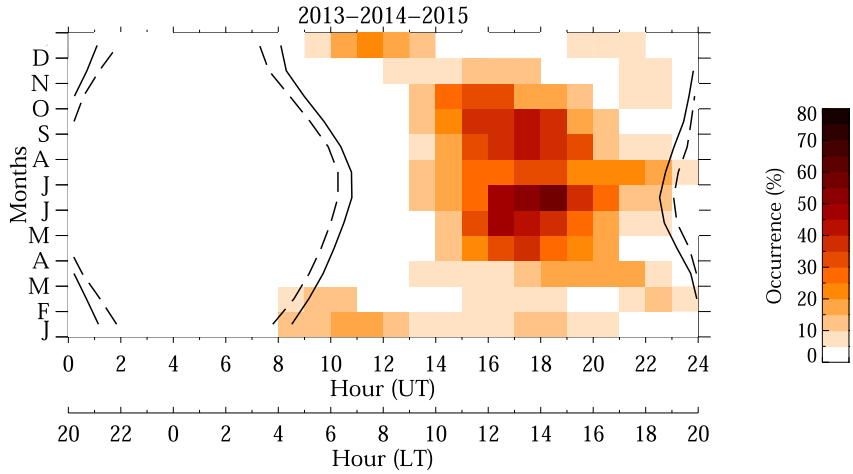

Figure 8. The occurrence rate for quiet-time daytime MSTIDs as a function of time observed at the Andean geomagnetic low latitudes. The black dashed-dot-dot-dot and dashed lines show the solar terminator at 110 and 300 km, respectively.

that the direction of propagation of the MSTIDs observed during the winter is the same as the direction of propagation of MSTIDs observed at geomagnetic equatorial latitude (see Figure 5c).

Figure 10 shows the propagation directions of daytime MSTIDs at the Andes geomagnetic low latitude as a function of time. During the winter (Figure 10c), MSTIDs propagate equatorward between 12 and 23 UT, and there is no change in the propagation direction over time. The same results are observed at geomagnetic equatorial

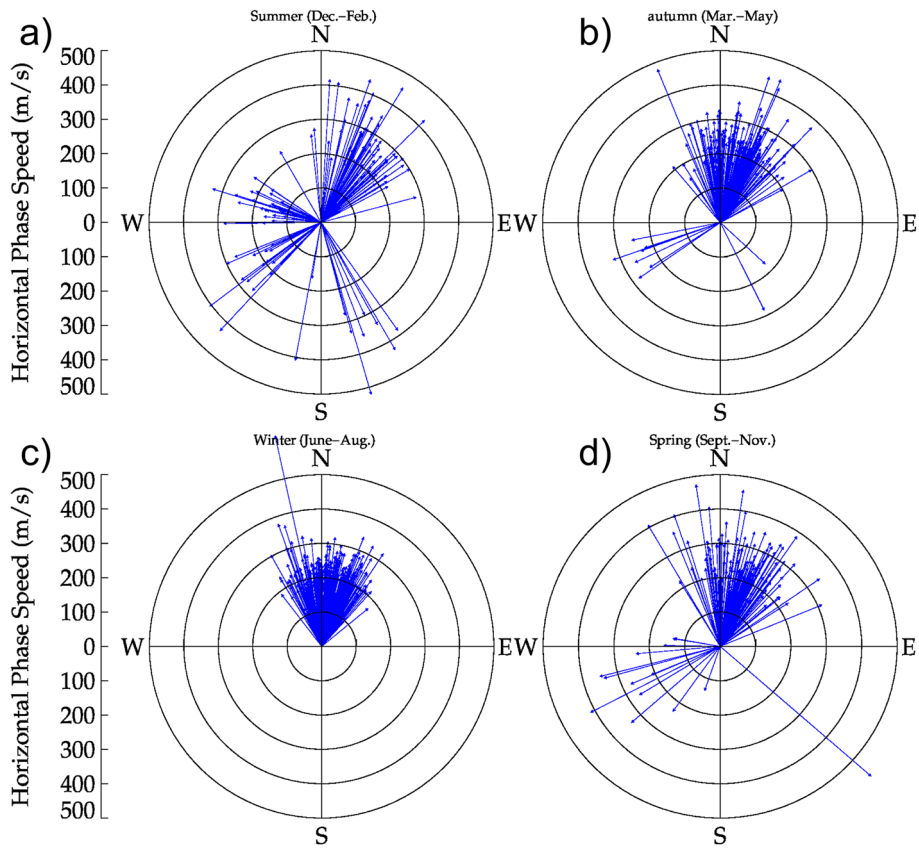

Figure 9. The propagation direction of quiet-time geomagnetic low latitudes daytime MSTIDs for (a) summer, (b) autumn, (c) winter, and (d) spring. Each circular line indicates a constant horizontal phase speed.

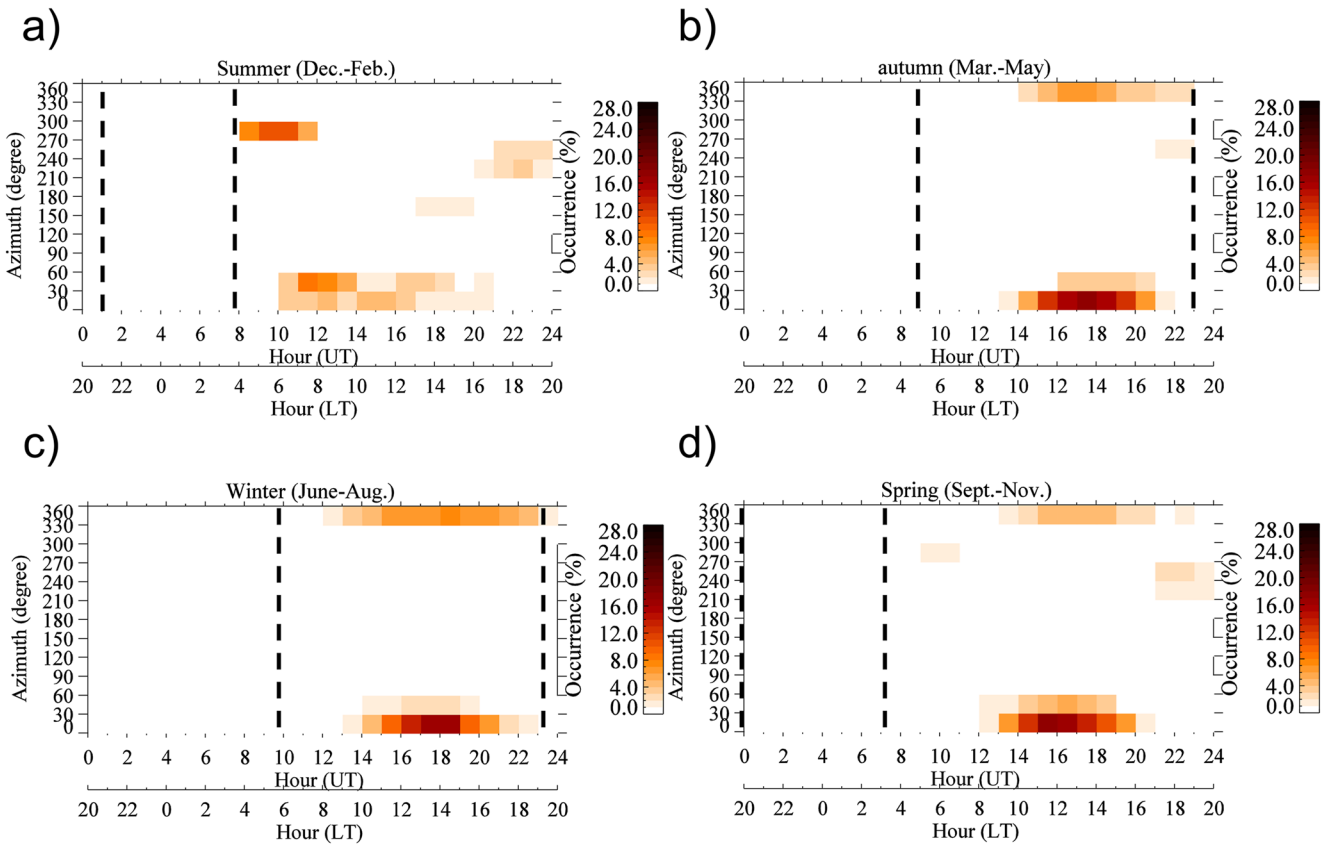

Figure 10. Local time dependency of the propagation direction of quiet-time daytime MSTIDs at geomagnetic low latitudes for (a) summer, (b) autumn, (c) winter, and (d) spring. The black dashed lines show the solar terminator.

latitudes (Figure 6c). On the other hand, during the summer (Figure 10a), it is observed that dawn MSTIDs (between 8 and 12 UT) propagate to the northwest and northeast. Moreover, between 12 and 17 UT the MSTIDs propagate to the north-northeast, and between 17 and 20 UT, the MSTIDs propagate both north-northeast and south-southeast. During autumn (Figure 10b), the propagation directions change with local time. The MSTIDs propagate equatorward between 13 and 22 UT. Near dusk (between 21 and 24 UT), their propagation directions are equatorward and southwestward. During the spring (Figure 10d), daytime MSTIDs have similar characteristics compared to autumn (Figure 10b). The only difference during spring is that the dawn MSTIDs propagate to the northwest.

4. Discussion

The focus of this study is to discuss the characteristics of the quiet-time daytime MSTIDs observed at the geomagnetic equatorial and low latitudes of the Andes Mountains. We also discussed the possible sources of the observed MSTIDs and compared the observed MSTIDs at geomagnetic equatorial and low latitudes. Finally, we compared our results with observations and numerical model results in the same region and in other parts of the world.

4.1. Daytime MSTID Propagation Direction

The daytime MSTID propagation directions may be helpful in indicating the possible geographical locations of their sources. This can change from one region to another. Thus, it is crucial to have observations in both hemispheres and at different latitudes and longitudes to understand the dynamics of the MSTIDs in the ionosphere. In this way, these observations will provide further details to the scientific community that could be included in numerical models to improve the predictability of the MSTIDs over South America.

4.1.1. Geomagnetic Equatorial Latitude Latitudes

In the southeast-southern part of Brazil, daytime MSTIDs have propagation directions that depend on the season (Figueiredo et al., 2018a). Daytime MSTIDs over the Andes Mountains propagate north-northeast and south-southwest during the autumn (from March to May) but propagate only toward the north-northeast during the winter (from June to August). For comparison, in the Asian sector, Chen et al. (2019) observed that daytime MSTIDs propagated to the southwest-west.

Figueiredo et al. (2018a) observed daytime MSTIDs over the southeast-southern part of Brazil propagating north-northeast and southeast-south-southwest during the autumn (from March to May). On the other hand, during the winter, they observed daytime MSTIDs propagating only to the north-northeast. In the present study, we find similar propagation directions over the Andes Mountains during autumn and winter (see Figures 5b and 5c) compared to Figueiredo et al. (2018a). During the summer, we find that the daytime MSTIDs propagate to the southeast-south and southwest-west, while on the East coast, the MSTIDs propagate in all directions (see Figure 8a of Figueiredo et al. (2018a)). During the spring, the only difference in the East and West sectors is that the daytime MSTIDs propagate to the southwest-west in the present study, while in the East sector; Figueiredo et al. (2018a) only observed 6 MSTIDs events propagating in this direction.

When we compare this present study with observations made in the Asian sector and the other regions in South America, it is clear that the propagation directions of the MSTIDs observed during the daytime are quite different. These results suggest that the sources of the waves in the present study are different than those in the Asian section. We will provide more details on this topic below in Section 4.2.

4.1.2. Geomagnetic Low Latitude Latitudes

Until now, daytime MSTIDs observed in the southern hemisphere at geomagnetic low latitudes have not yet been reported; thus, we cannot compare our results with previous works. It is observed that daytime MSTIDs at geomagnetic low latitudes propagate mostly north-northeast (∼60%). Nevertheless, we note that the daytime MSTID propagation directions are different during the December solstice (summer) and equinoxes. During the December solstice, the daytime MSTIDs propagate in almost all directions with a preference for northeastward. On the other hand, MSTIDs during the equinox months propagate to the north, northeast, and southwest but the majority propagate north-northeast. During the June solstice (winter), the daytime MSTIDs observed at geomagnetic equatorial and low latitudes propagate equatorward.

Otsuka (2021) suggests that MSTIDs that move mainly toward the equator are caused by the interaction between ions and neutral particles in the ionosphere. This is because the ions can move along the magnetic field lines more easily than across them, due to their high gyrofrequency compared to their collision frequency in the ionosphere. Besides, the collision frequency is responsible for moving the ions to directions perpendicular to the magnetic field line. Consequently, these ions would be trapped in the magnetic field and propagate more easily along the magnetic field line.

Another observed characteristic of our results is that daytime MSTIDs have different propagation directions during the summer and equinoxes as compared to observations in the northern hemisphere at middle latitudes and different longitudes. For comparison, Kotake et al. (2007) and Otsuka et al. (2011) observed that daytime MSTIDs propagate southeast-south-southwest (equatorward) during the summer at mid-latitudes. However, in the present study, daytime MSTIDs propagate in all directions during the summer, although the northeastward propagation direction is preferred, which has some agreement with those studies. On the other hand, during the equinox, our results find that the daytime MSTIDs propagate to the north-northeast and south-southwest directions. Whereas Kotake et al. (2007) and Otsuka et al. (2011) found during the equinox that the daytime MSTIDs propagate predominantly southeastward. They also reported that the propagation direction changed from southeastward to southwestward over time. The only similarity between the present study and Kotake et al. (2007) during the equinox season is that most of the TIDs were propagating toward the equator, which is likely due to the source being near the polar region, which will be discussed in the following section.

Regarding daytime MSTIDs observed between 08:00 and 12:00 UT at the geomagnetic low latitude during the summer, we observe in Figure 10a that most of the MSTIDs propagated in two distinct directions: west-northwest (78%) and north-northeast (17%). These two propagation directions are almost perpendicular to each other. Additionally, the MSTIDs that move toward the west-northwest and the north-northeast have similar horizontal phase

speeds (i.e., between 100 and 360 m/s). The difference in the propagation direction of these MSTIDs indicates that they have different origins and physical mechanisms. On the other hand, Otsuka et al. (2011) and Tsugawa et al. (2007) observed that dawn MSTIDs propagate to the northeast-east over Japan. Otsuka et al. (2011) argued that the wind filtering mechanism might be responsible for MSTIDs propagating in a specific direction. Using the Horizontal Wind Model 14 (Drob et al., 2015), a simulation of the neutral wind at 250 km altitude, 70°W; 36°S, and between 8 and 12 UT was made to study the characteristics of the wind. The model results showed that the wind direction varied from 314 to 355° (not shown). Our observations also detected MSTIDs with propagation directions between 270 and 330°, which were almost in the same direction as the neutral wind. However, TIDs have a larger horizontal phase speed than the wind speed and are not filtered by the wind. Besides, this result is different from other results, which show that GWs tend to propagate nearly opposite to the direction of the wind (Becker et al., 2022; Crowley & Rodrigues, 2012).

Comparing the propagation direction of daytime MSTIDs between geomagnetic equatorial and low latitudes, we observe similarities only during the winter. These MSTIDs propagate toward the equator. This may be in part because the horizontal wind component of the diurnal tide in the thermosphere is oriented toward the poles at LT noon (e.g., Roble & Ridley, 1994), and the gravity waves (GWs) which best survive dissipation by molecular viscosity in the thermosphere propagate approximately opposite to the background wind (e.g., Crowley & Rodrigues, 2012; Fritts & Vadas, 2008; Miyoshi et al., 2018). Our results, therefore, support these previous results. On the other hand, during the equinox, the MSTIDs in geomagnetic low latitudes propagate mainly toward northwest-north-northeast, while MSTIDs in geomagnetic equatorial latitudes propagate toward northwest-north-northeast and southeast-south-southwest. Finally, during the summer, MSTIDs observed in geomagnetic low latitudes propagate in all directions. In contrast, geomagnetic equatorial latitudes of MSTIDs propagate only toward the south and southeast. Therefore, analyzing both latitude regions during the summer and equinox, we observe that the source locations of MSTIDs are different and depend on the season.

4.2. Possible Sources of Daytime MSTIDs Observed Over the Andes Mountains at Geomagnetic Equatorial and Low Latitudes

In the previous section, we found that the MSTIDs have specific propagation directions for each season; these results could help us to associate the sources of these MSTIDs. Figueiredo et al. (2018a) used cloud top brightness temperature (CTBT) maps from the Geostationary Operational Environmental Satellite System 13 (GOES 13) to determine the location of tropospheric deep convection between 2013 and 2015. The authors observed that the daytime MSTIDs propagate in all directions at the equinoxes and summer solstice. Figueiredo et al. (2018a) suggested that the GWs are generated by deep convection and propagate into the thermosphere/ionosphere.

A closer analysis of Figures 10a, 10b, and 10d of Figueiredo et al. (2018a) shows that deep convection during the summer and equinoxes occur in the north and east sectors of the Chilean and Argentinian Andes Mountains (geographic: 15–30°S and 30–45°S; 70°W). During the summer solstice and equinoxes, the MSTIDs propagate southeast, south, and southwestward at geomagnetic equatorial latitudes of the Andes Mountains. Marengo (2004) analyzed rainfall climatology in the Amazon basin, where they observed that the beginning of the rainy season is at the end of September, while the end of the rainy season is in early June. Also, the rainy season in northwestern and central-western Argentina is between October and March (Agosta & Compagnucci, 2012; Oncken et al., 2006). Therefore, the propagation direction of the daytime low-latitude MSTIDs over Chile and Argentina, during the middle of spring (October) to the beginning of winter (June), that propagate southeast, south, and southwestward agree with the rainy period in the Amazon basin.

On the other hand, at geomagnetic low latitudes, the daytime MSTIDs that propagate to the southwest might be related to the rainy season (the end of spring (November), summer (December, January, and February), and beginning of autumn (March)) in the northwestern and central-western region of Argentina. Hoffmann et al. (2013) observed GWs in the stratosphere based on 9 years (2003–2009) of data collected by the Atmospheric Infrared Sounder (AIRS) aboard NASA's Aqua satellite. The authors observed that in South America, daytime GWs are generated in different regions according to the season. In the summer, they are strongly generated in southern Brazil, Paraguay, and northeastern Argentina and slightly generated over the Antarctic Peninsula and the southern Andes. Also, daytime GWs are generated over the Antarctic Peninsula and the southern and northern Andes in the equinox months. Therefore, the propagation direction of the MSTIDs to the north, northeast, and southwest during equinox and summer corroborates the hot spots of GWs in the stratosphere observed by Hoffman et al. (2013).

During the daytime winter, the MSTIDs we observe here propagate in different directions compared to the other seasons because they are predominately northward. Indeed, daytime MSTIDs are observed almost every single day during this season. Figure 11 shows the average zonal wind at 5 km altitude during the summer, autumn, winter, and spring at 06:00 UT in the South American Continent for 2013 (a), 2014 (b), and 2015 (c) using data from the Modern-Era Retrospective analysis for Research and Applications version 2 (MERRA-2) (R. Gelaro, et al., 2017). During the summer, the zonal wind blows eastward (positive values) at high geographic latitudes (>45°S). On the other hand, during the autumn, the zonal wind is not strong in the Andes Mountains. Besides, during the winter and spring, the zonal wind blows eastward at geographic middle to high latitudes (from 30 to 55°S). Also, it is more intense in the Andes Mountains sector (from 65 to 75°W). Therefore, this eastward wind flow over the mountains must have generated mountain waves. Hoffmann et al. (2013) observed stratospheric hotspot GWs over the southern Andes and the Antarctic Peninsula; these GWs are mountain waves excited from wind flow over the mountains (Alexander & Teitelbaum, 2007; Hoffmann et al., 2013, 2016; Kruse et al., 2022). Also, Sivakandan et al. (2021) suggest that mountain waves launched from the Andes Mountains could increase GW activities resulting in high daytime MSTID activities over South America. The present observation agrees with the observations of Sivakandan et al. (2021).

Vadas et al. (2019) observed 17 Traveling Atmospheric Disturbances (TADs) at 277 km altitude using the satellite Gravity Field and Ocean Circulation Explorer (GOCE) over the Andes Mountains during a geomagnetically-quiet period when "hotspot" GWs were present over the Southern Andes. The TADs had wavelengths between 170 and 1,850 km, intrinsic periods between 11 and 54 min, and intrinsic horizontal phase speeds of 245–630 m/s. Using reverse ray tracing, they found that nearly all of the GWs must have been generated in the thermosphere and that the most likely source for the primary GWs was mountain waves excited by wind flow over the Andes Mountains. Vadas and Becker (2019) analyzed the results from a global circulation model (GCM) in the South American winter time during a mountain wave event over the Southern Andes and found that the mountain waves break in the stratosphere, thereby depositing momentum into the background flow and creating local body forces (i.e., local horizontal accelerations). These body forces generated secondary GWs propagating up to the MLT before breaking or dissipating from critical level filtering or molecular viscosity. This process again resulted in the creation of local body forces, which generated medium- and large-scale tertiary GWs with concentric ring structures. These tertiary GWs propagated in all directions except perpendicular to the force direction. Also, Vadas and Becker (2019) showed that concentric tertiary GWs with the highest amplitudes mainly propagate northeastward and southwestward. Moreover, the authors found that GWs traveling southwestward reach critical levels due to wind and attenuate due to molecular viscosity. This present study observed that daytime MSTIDs usually propagate north-northeast. Furthermore, the research conducted by Vadas and Becker (2019) pointed out that certain tertiary gravity waves were observed to propagate over Brazil (see Figure 1 of that work). Besides, the authors noted that some of these waves had exceptionally large horizontal phase speeds >400 m/s and propagated up to the model top (z = 200 km). Therefore, these findings were consistent with both simulation results and observational data.

Negale et al. (2018) studied daytime MSTIDs for 3 years in Fairbanks, Alaska, USA. They found that the observed MSTIDs had the following characteristics: horizontal wavelengths ranging from 369 to 514 km; periods between 37 and 44 min; and horizontal phase speeds ranging from 155 to 212 m/s. During the winter, the authors noted that the propagation direction of the MSTIDs was southward (equatorward), which is opposite to the direction of the diurnal tide in the thermosphere. The initial source of these waves could have been mountain waves generated by the Brooks Range Mountains north of Fairbanks, which dissipated in the stratosphere and generated secondary GWs, which then dissipated in the MLT and generated tertiary GWs. In the present study, the MSTID propagation direction is toward the north-northeast (equatorward as well, again opposite to the daytime diurnal tide direction). However, the horizontal phase speed in the present study is significantly higher than that reported by Negale et al. (2018). Fast GWs can avoid dissipation from molecular viscosity in the lower thermosphere and propagate into the middle thermosphere (F region) before dissipating (Vadas, 2007). Note that these GWs tend to have longer horizontal wavelengths (Figures 3e and 7e) and, therefore, travel longer horizontal distances while propagating to the mid and upper thermosphere. Since most of the propagation directions of the MSTIDs we observed at low and middle latitudes are opposite to the direction of the neutral wind, our observed MSTIDs have higher intrinsic phase speeds than the observed phase speeds.

Furthermore, ∼50% of the observed MSTIDs have observed phase speeds greater than 250 m/s. As mentioned previously, all MSTIDs propagate north and northeast during the winter. Using HWM14, the daytime neutral wind

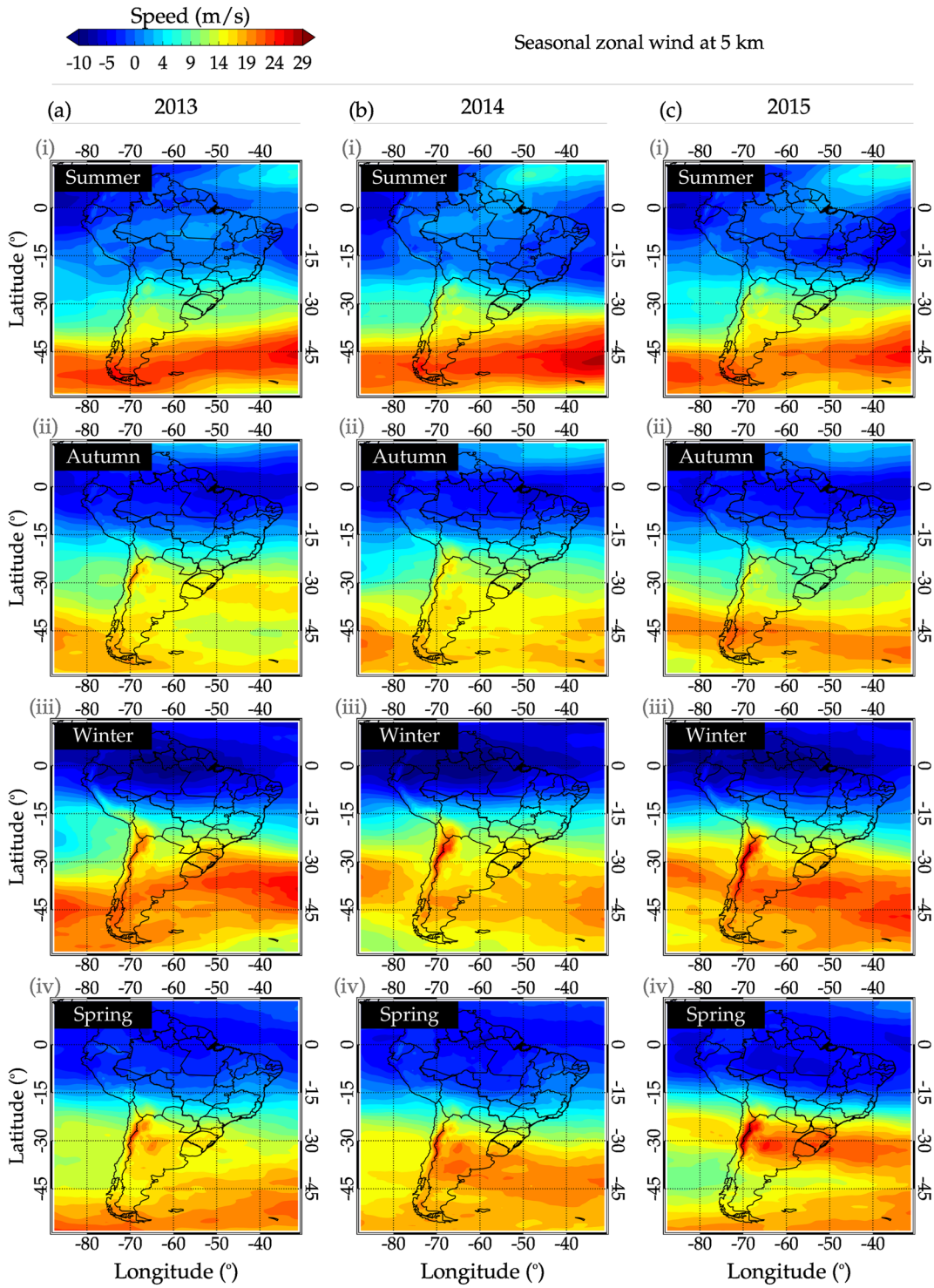

Figure 11. The average zonal wind component from MERRA-2 at 5 km altitude at 06:00 UT for 2013 (a), 2014 (b), and 2015 (c) during summer, autumn, winter, and spring. Positive zonal wind denotes eastward.

during the winter is south-southwestward, with a magnitude of ~50 m/s at 250 km altitude (Drob et al., 2015). Thus, the intrinsic phase speed of the MSTIDs will be ~50 m/s higher than the observed phase speed. Therefore, based on the works of Vadas et al. (2019), Vadas and Becker (2019), and Becker and Vadas (2020), the daytime winter MSTIDs observed propagating approximately northward (from the approximate vicinity of the Andes

Mountains) were mostly likely tertiary (or high order) GWs generated in the thermosphere. On the other hand, if a GW propagates in the same direction as the neutral wind, this wave will have a shorter vertical wavelength and dissipate at a lower altitude because molecular viscosity will have a stronger effect on it (Vadas, 2007). In this way, the wind filtering mechanism is also important for controlling the propagation direction of MSTIDs. However, our results cannot be only due to neutral wind filtering because, during the daytime, northward-propagating waves are most prominent during the autumn, winter, and spring, when the polar night jet is prominent. Polar vortex and mountain waves created by wind flow over the Andes Mountains break in the stratosphere or mesosphere.

It is well-known that there is a prominent GW winter hotspot seen in the GOCE and CHAMP satellites at $z = 250$–400 km over the Southern Andes and Antarctica Peninsula at $z \sim 250$–450 km (Forbes et al., 2016; Liu et al., 2017; Park et al., 2014; Trinh et al., 2018). However, because mountain waves cannot propagate to these heights due to breaking and dissipation, the source of these GWs was unknown. Using the HIAMCM extended to $z = 450$ km, Becker and Vadas (2020) showed that these hotspot wintertime GWs were composed of tertiary (and higher-order) GWs from orographic forcing. They also found that the longer-horizontal wavelength GWs propagated further from the Andes than the small-medium-scale GWs. This result was confirmed by a detailed analysis of individual TADs in GOCE and CHAMP satellite data (Xu et al., 2021). Because these hotspot GWs perturb the ionosphere while they propagate through the thermosphere via neutral-ion collisions, it is expected that they would create MSTIDs. Therefore, based on these previous studies and all of the evidence discussed in this study, we conclude that most of the quiet-time and winter daytime MSTIDs we observe propagating to the north-northeast direction are likely tertiary (or higher-order) GWs from orographic forcing.

The MSTIDs observed in the geomagnetic low latitudes latitude between 08:00 and 12:00 UT during summer could be generated by the solar terminator due to the density gradient and pressure generated in the transition from night to day. Figure 2 shows that this type of wave is generated 1–2 hr after the passage of the dawn solar terminator and that the MSTID has a propagation direction that follows the solar terminator. Forbes et al. (2008) discuss GWs generated by solar terminators moving at subsonic speed (450 m/s) with a spatial scale and period of order of 1,000 km and 30 min, respectively. In addition, they mentioned that small-scale waves are frequently seen during this time occurrence. Therefore, our results agree well with that of Forbes et al. (2008). On the other hand, daytime MSTIDs between 8:00 and 12:00 UT that propagate to the north-northeast are probably due to GWs generated by other sources. Further studies would be needed for a better understanding of these MSTIDs.

4.3. Daytime MSTIDs Characteristics in Geomagnetic Equatorial and Low Latitudes

Many studies on MSTIDs have been conducted at geomagnetic equatorial and low latitudes (e.g., Ding et al., 2011; Frissel et al., 2014; Ishida et al., 2008; Kotake et al., 2007; Negale et al., 2018; Otsuka et al., 2011, 2013; Shiokawa et al., 2003). However, only a few works have reported findings over the Andes Mountains (e.g., Duly et al., 2013; Martinis et al., 2006; Sivakandan et al. (2021)). In addition, Alexander et al. (2015) observed oscillations in COSMIC radio occultation density GPS profiles between 1 July 2006, and 31 December 2013, in the Andes region. The authors observed that the highest ionospheric oscillations occur in the eastern part of the Andes Mountain range during the winter.

In the present study, the daytime MSTIDs at geomagnetic equatorial latitudes have an average horizontal wavelength, horizontal phase speed, and period of 589 ± 170 km, 288 ± 74 m/s, and 35 ± 7 min, respectively. The daytime MSTIDs observed in the Southeast-South of Brazil have 445 ± 107 km, 323 ± 81 m/s, and 24 ± 4 min, respectively (Figueiredo et al., 2018a). Thus, the horizontal wavelength and period at geomagnetic equatorial latitudes over the Andes are larger than in the Southeast-South of Brazil. On the other hand, in the southeast-south of Brazil, the MSTIDs are faster than those over the Andes. Also, TIDs over the Andes are more frequent (13%) than TIDs over southeast-south of Brazil. Numerical simulations and more observations are needed to see the influence of South Atlantic magnetic anomaly or other physical phenomena that affect this occurrence of TIDs and its parameters in Brazil.

When we compare the daytime MSTIDs observed in the South American sector to the Asian sector at geomagnetic equatorial latitudes, we find that the seasonality (spring, autumn, and winter), and time of occurrence (from 10 to 17 local time) are similar. Also, the studies in the Asian sector (e.g., Chen et al. (2019)) did not associate these characteristics as being due to tertiary waves from mountain wave breaking. However, there are significant differences in the other parameters of the daytime MSTIDs. Our results show that the wavelengths and phase

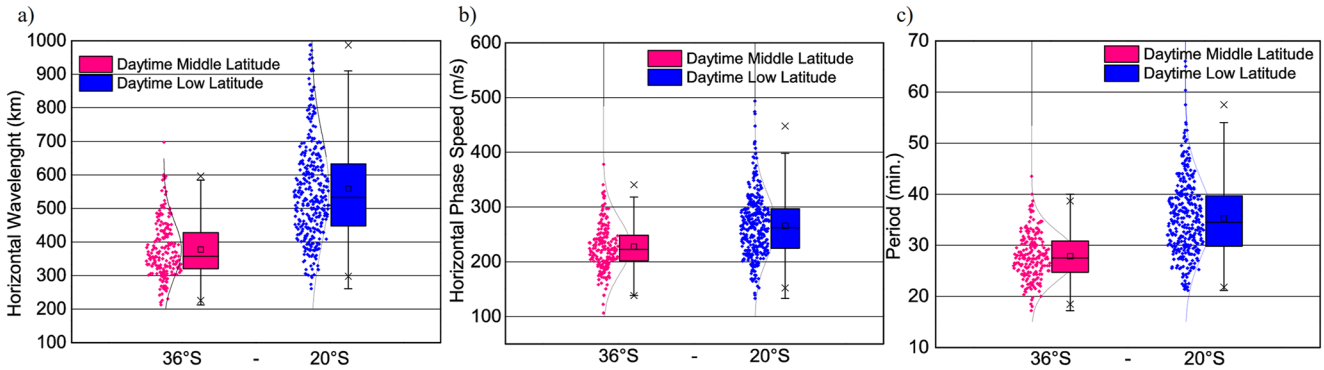

Figure 12. Boxplots of the horizontal wavelength (a), horizontal phase speed (b), and period (c) of daytime MSTIDs observed at the geomagnetic low (geographic middle 36°S—pink) and geomagnetic equatorial (geographic low 20°S—blue) latitudes over the Andes Mountains when Kp ≤ 3 during the winter months. The box and horizontal line inside the interquartile range are mean and median, respectively.

speeds (589 ± 170 km; 288 ± 74 m/s) are greater than those observed (250–400 km; 120–240 m/s) by Chen et al. (2019). One possible explanation related to the different horizontal wavelengths between South American and Asia sectors could be the thickness of the magnetic flux tube. The magnetic flux tubes are narrower in the northern hemisphere than in the southern hemisphere. Consequently, the horizontal wavelength in the southern hemisphere is larger than in the northern hemisphere because the ions move along the magnetic field lines.

In the present study, we compared the characteristics of MSTIDs in geomagnetic equatorial and low latitudes. Figure 12 contains three boxplots showing the horizontal wavelength (a), horizontal phase speed (b), and observed period (c) of the daytime MSTIDs during the winter months (JJA) at geomagnetic equatorial and low latitudes. The average horizontal wavelength, horizontal phase speed, and observed period of the daytime MSTIDs at geomagnetic low latitudes are 337 ± 83 km (559 ± 161 km), 228 ± 50 m/s (266 ± 57 m/s), and 28 ± 5 min (35 ± 8 min), respectively. A characteristic of the MSTIDs observed at geomagnetic low latitudes is that the horizontal wavelength, horizontal phase speed, and observed period are averagely smaller than those observed at geomagnetic equatorial latitudes over the Andes Mountains.

The dependence of the MSTIDs characteristics on latitude (distance from the source) during the daytime in Figure 12 is further evidence that these MSTIDs are created by tertiary (or higher order) GWs generated from local body forces in the thermosphere. Indeed, GWs with larger wave periods have propagation angles closer to the horizontal and reach a certain altitude (z) further from the source than GWs with smaller wave periods. These former GWs with larger periods also tend to have larger horizontal wavelengths (e.g., Vadas & Crowley, 2010). Vadas and Becker (2019) observed that at any given time, the GW horizontal wavelength increases as the radius squared ($\sim R^2$) from the center of the force (see also Vadas & Azeem, 2020). This is due to the fact that GWs observed simultaneously from the same body force have the same vertical group velocity, which implies that those GWs with larger periods have larger horizontal wavelengths (i.e., the larger radius at the observation altitude). However, the present study did not show good agreement with the horizontal wavelength being proportional to the radius squared from the center of the force; this is likely due to the lack of sufficient data with radii (there are only two observational locations).

Another difference between daytime MSTIDs at geomagnetic equatorial and low latitudes is the time of occurrence. At geomagnetic low latitudes, MSTIDs have a peak occurrence between 11:00 and 16:00 LT. On the other hand, MSTIDs at geomagnetic equatorial latitudes have a wide time of occurrence, but the highest occurrence of MSTIDs is from the end of the morning to near sunset (from 10:00 to 18:00 LT). This suggests that MSTIDs could be an important contributor to the generation of plasma bubbles in the region near the magnetic equator (e.g., Takahashi et al., 2018, 2020, 2021). In addition, Grocott et al. (2013) observed MSTIDs over the Antarctic Peninsula using the High-Frequency radar. They observed that daytime MSTIDs are more frequent between 09:00 and 13:00 LT. This observation suggests that the times of occurrence of MSTIDs observed at geomagnetic equatorial and low latitudes may be associated with the origin of these waves either to be over the Antarctic Peninsula or the Andes Mountains.

Finally, the occurrence rate of MSTIDs is higher (25%) at geomagnetic equatorial latitudes than at geomagnetic low latitudes. This difference is mainly associated with MSTIDs propagating toward the southeast, south,

and southwest (141 events at geomagnetic equatorial latitudes against 24 events at geomagnetic low latitudes). These differences associated with occurrence rate may be related to the Amazon basin because it is next to the geomagnetic equatorial latitude region, where deep convection may likely excites many of these Gravity waves that eventually induce MSTIDs. Also, deep convection can cause the excitation of high-frequency gravity waves (Alexander & Pfister, 1995), thus, they propagate very close to the vertical and do not propagate very far horizontally (Vadas, 2007). Such gravity waves would then be observed mainly at geomagnetic equatorial latitudes rather than geomagnetic low latitudes. Also, the MSTIDs observations were made in the Equatorial ionization Anomaly (EIA) region. The EIA is generated by ascending plasma in the magnetic equator due to the $\mathbf{E} \times \mathbf{B}$ drift. Thus, the plasma in high altitudes diffuses along the magnetic field lines. Consequently, it creates crests in both hemispheres with an accumulation of plasma within $\sim\pm 20^{\circ}$ geomagnetic latitudes and altitudes ranging from 300 to 600 km (Balan et al., 2018). As the effect on the daytime MSTIDs, the ion drag (neutral-ion collision frequency) could dissipate the MSTIDs or reduce the gravity wave amplitudes. Based on the present study, the EIA probably affects vertical and horizontal propagation of the MSTIDs more in the geomagnetic low latitude (from -20 to -30°) than in equatorial latitude (from 0 to -15°) because the molecular and kinematic viscosity increases in the EIA region. In addition, it is important to mention that MSTIDs could not propagate higher than 300 km altitude due to dissipative effects associated with EIA.

5. Conclusions

We have investigated the characteristics of daytime MSTIDs observed at *geomagnetic equatorial and low latitudes* of the Andes Mountains during geomagnetic quiet time ($Kp \leq 3$) using detrended TEC keograms for 3 years from 2013 to 2015. We found that the characteristics and time occurrence of the MSTIDs are different in these regions. The observed characteristics are summarized as follows:

At *geomagnetic equatorial latitudes*, 946 MSTIDs were observed with the following characteristics: horizontal wavelengths of 589 ± 170 km, horizontal phase speeds of 288 ± 74 m/s, and observed periods of 35 ± 7 min. The highest occurrence of MSTIDs was during the winter (JJA) and equinox (MAM-SON) months. The occurrence time of the MSTIDs depends on the season. During the winter and equinoxe months, the MSTIDs occur throughout the afternoon, while in summer (DJF), the MSTIDs occur in the late afternoon and early evening. The propagation directions of the MSTIDs during the solstices have the following characteristics. In the summer, the MSTIDs propagate southeast, south, southwestward, and west. In the winter, the MSTIDs propagate northwest, north, and northeastward with the following characteristics: horizontal wavelengths of 556 ± 158 km, horizontal phase speeds of 268 ± 58 m/s, and periods of 35 ± 7 min. During the equinoxes, the MSTIDs propagate north, south, southwestward, and west.

1. At geomagnetic low latitudes, 726 daytime MSTIDs were observed most frequently during the winter and at the equinox months. They have average horizontal wavelengths of 436 ± 139 km, periods of 31 ± 7 min, and phase speeds of 241 ± 65 m/s. The propagation direction depends on the season: in the summer, they propagate in almost all directions, with the dominant propagation direction in the north-northeast. In the winter, they propagate exclusively north-northeastward. During the equinoxes, they propagate north-northeast and southwestward. Additionally, the daytime MSTIDs observed between 8:00 and 12:00 UT occur in the late spring and summer. They have wavelengths of 242–1,172 km, periods of 23–60 min, and phase speeds of 74–460 m/s. Also, the propagation directions of these MSTIDs are west-northwest and north-northeastward. These MSTIDs that propagate west-northwestward are probably generated from the passage of the solar terminator that generates a density and pressure gradient in the transition from night to day.
2. The horizontal wavelength and horizontal phase speed of the MSTIDs at geomagnetic equatorial latitudes (589 ± 170 km and 288 ± 74 m/s) are greater than those at geomagnetic low latitudes (436 ± 139 km and 241 ± 65 m/s). During the winter, this is likely due to the thermospheric body forces from orographic forcing and mountain wave breaking over the Southern Andes and Antarctica Peninsula, since the wavelength and phase speed increase with distance from the source. To gain more insights into the atmospheric GWs propagation in different seasons, numerical simulations should be performed for various seasonal scenarios.
3. The daytime MSTIDs at geomagnetic equatorial latitudes that propagate southeast, south, or southwestward agree well with the rainy season in the Amazon basin. On the other hand, the daytime MSTIDs at geomagnetic low latitudes that propagate southwest, west, or northwestward may be related to the rainy season in Argentina's northwestern and central-western regions. On the other hand, the wintertime daytime MSTIDs

at geomagnetic equatorial and low latitudes propagate north and northeastward. This direction is opposite to the background wind, implying there is the occurrence of wind filtering. Additionally, this shows that the sources of the underlying GWs are at high latitudes in South America (likely mountain wave breaking over the Antarctic Peninsula and the Andes Mountains region).

4. Due to the sound speed value below the altitude of 100 km, 56% and 25% of wintertime daytime MSTIDs observed over the Andes Mountains at geomagnetic equatorial and low latitudes, respectively, have horizontal phase speeds >250 m/s, and, hence, the thermosphere is the most likely source of these waves. Moreover, this conclusion applies to other seasons when MSTIDs exhibit horizontal phase speeds above 250 m/s. The underlying GWs are most likely tertiary or high-order GWs created in the thermosphere via multi-step vertical coupling from mountain waves breaking far below during the winter.

Data Availability Statement

The GPS data used in this study were freely provided by the servers of UNAVCO servers https://observablehq.com/@earthscope/gnss-data-access.

Acknowledgments
The present work was supported by Fundação de Amparo à Pesquisa do Estado de São Paulo (FAPESP) project no 2018/09066-8 and 19/22548-4. C. A. O. B. Figueiredo thanks Fundação de Apoio a Pesquisa do Estado da Paraíba (FAPESQ). SLV was supported by NSF Grant AGS-1832988 and by NASA Grant 80NSSC19K0836. Thanks to the Brazilian Ministry of Science, Technology and Innovation (MCTI) and the Brazilian Space Agency (AEB) who supported the present work under the Grants PO 20VB.0009. The present work was supported by CNPq (Conselho Nacional de Pesquisa e desenvolvimento) under the Grants 305461/2015-0, 307653/2017-0, 300974/2020-5, 303511/2017-6, 301670/2023-4. K. Shiokawa and Y. Otsuka are also thankfull for the support by JSPS (Japan Society for Promotion of Science) KAKENHI (Grant JP 15H05815). P. K. Nyassor thanks Fundação de Amparo à Pesquisa do Estado de São Paulo (FAPESP) under the process number 2021/07491-6. The authors would like to thank Dr. Joe Huba for his helpful comments regarding this manuscript. Also, the authors are grateful to Dr. Michelli Barros for her valuable guidance on the statistical analysis.

References

Agosta, E. A., & Compagnucci, R. H. (2012). Central-West Argentina summer precipitation variability and atmospheric teleconnections. *Journal of Climate*, *25*(5), 1657–1677. https://doi.org/10.1175/JCLI-D-11-00206.1

Alexander, M. J., & Fritts, D. C. (2003). Gravity wave dynamics and effects in the middle atmosphere. *Reviews of Geophysics*, *41*(1), 1003. https://doi.org/10.1029/2001RG000106

Alexander, M. J., & Pfister, L. (1995). Gravity wave momentum flux in the lower stratosphere over convection. *Geophysical Research Letters*, *22*(15), 2029–2032. https://doi.org/10.1029/95gl01984

Alexander, M. J., & Teitelbaum, H. (2007). Observation and analysis of a large amplitude mountain wave event over the Antarctic Peninsula. *Journal of Geophysical Research*, *112*(D21), D21103. https://doi.org/10.1029/2006JD008368

Alexander, P., De la torre, A., Schmidt, t., Llamedo, p., & Hierro, r. (2015). Limb sounders tracking topographic gravity wave activity from the strato-sphere to the ionosphere around midlatitude Andes. *Journal of Geophysical Research: Space Physics*, *120*(10), 9014–9022. https://doi.org/10.1002/2015JA021409

Amorim, D. C. M., Pimenta, A. A., Bittencourt, J. A., & Fagundes, P. R. (2011). Long term study of medium-scale traveling ionospheric disturbances using oi 630 nm all sky imaging and ionosonde over Brazilian low latitudes. *Journal of Geophysical Research*, *116*(A6), A06312. https://doi.org/10.1029/2010JA016090

Azeem, I., Vadas, S. L., Crowley, G., & Makela, J. J. (2017). Traveling ionospheric disturbances over the United States induced by gravity waves from the 2011 Tohoku tsunami and comparison with gravity wave dissipative theory. *Journal of Geophysical Research: Space Physics*, *122*(3), 3430–3447. https://doi.org/10.1002/2016JA023659

Azeem, I., Yue, J., Hoffmann, L., Miller, S. D., Straka, W. C., & Crowley, G. (2015). Multisensor profiling of a concentric gravity wave event propagating from the troposphere to the ionosphere. *Geophysical Research Letters*, *42*(19), 7874–7880. https://doi.org/10.1002/2015GL065903

Balan, N., Liu, L., & Le, H. (2018). A brief review of equatorial ionization anomaly and ionospheric irregularities. *Earth and Planetary Physics*, *2*(4), 257–275. https://doi.org/10.26464/epp2018025

Becker, E., Goncharenko, L., Harvey, V. L., & Vadas, S. L. (2022). Multi-step vertical coupling during the January 2017 sudden stratospheric warming. *Journal of Geophysical Research: Space Physics*, *127*(12), e2022JA030866. https://doi.org/10.1029/2022ja030866

Becker, E., & Vadas, S. L. (2018). Secondary gravity waves in the winter mesosphere: Results from a high-resolution global circulation model. *Journal of Geophysical Research: Atmospheres*, *123*(5), 2605–2627. https://doi.org/10.1002/2017jd027460

Becker, E., & Vadas, S. L. (2020). Explicit global simulation of gravity waves in the thermosphere. *Journal of Geophysical Research: Space Physics*, *125*(10), e2020JA028034. https://doi.org/10.1029/2020JA028034

Bevington, P., & Robinson, D. K. (2003). Error analysis. In *Data reduction and error analysis for the physical sciences* (Vol. 31, pp. 36–46). McGraw-Hill.

Bolmgren, K., Mitchell, C., Bruno, J., & Bust, G. S. (2020). Tomographic imaging of traveling ionospheric disturbances using GNSS and geostationary satellite observations. *Journal of Geophysical Research: Space Physics*, *125*(3), e2019JA027551. https://doi.org/10.1029/2019JA027551

Chen, G., Zhou, C., Liu, Y., Zhao, J., Tang, Q., Wang, X., & Zhao, Z. (2019). A statistical analysis of medium-scale traveling ionospheric disturbances during 2014–2017 using the Hong Kong CORS network. *Earth Planets and Space*, *71*(1), 52. https://doi.org/10.1186/s40623-019-1031-9

Crowley, G., & Rodrigues, F. S. (2012). Characteristics of traveling ionospheric disturbances observed by the TIDDBIT sounder. *Radio Science*, *47*(04), 1–12. https://doi.org/10.1029/2011RS004959

De la Torre, a., Alexander, p., Llamedo, p., Hierro, r., Nava, b., Radicella, s., et al. (2014). Wave activity at ionospheric heights above the Andes Mountains detected from FORMOSAT-3/COSMIC GNSS radio occultation data. *Journal of Geophysical Research*, *119*(3), 2046–2051. https://doi.org/10.1002/2013JA018870

Ding, F., Wan, W., Xu, G., Yu, T., Yang, G., & Wang, J. (2011). Climatology of medium-scale traveling ionospheric disturbances observed by a GPS network in central China. *Journal of Geophysical Research*, *116*(A9), A09327. https://doi.org/10.1029/2011JA016545

Drob, D. P., Emmert, J. T., Meriwether, J. W., Makela, J. J., Doornbos, E., Conde, M., et al. (2015). An update to the Horizontal Wind Model (HWM): The quiet time thermosphere. *Earth and Space Science*, *2*(7), 301–319. https://doi.org/10.1002/2014EA000089

Duly, T. M., Chapagain, N. P., & Makela, J. J. (2013). Climatology of nighttime medium-scale traveling ionospheric disturbances (MSTIDS) in the Central Pacific and South American sectors. *Annales Geophysicae*, *31*(12), 2229–2237. https://doi.org/10.5194/angeo-31-2229-2013

Essien, P., Figueiredo, C. A. O. B., Takahashi, H., Klutse, N. A. B., Wrasse, C. M., Afonso, J. M. D. S., et al. (2022). Intertropical convergence zone as the possible source mechanism for southward propagating medium-scale traveling ionospheric disturbances over South American low-latitude and equatorial region. *Atmosphere*, *13*(11), 1836. https://doi.org/10.3390/atmos13111836

Essien, P., Figueiredo, C. A. O. B., Takahashi, H., Wrasse, C. M., Barros, D., Klutse, N. A. B., et al. (2021). Long-term study on medium-scale traveling ionospheric disturbances observed over the South American Equatorial Region. *Atmosphere*, *12*(11), 1409. https://doi.org/10.3390/atmos12111409

Figueiredo, C. A. O. B., Takahashi, H., Wrasse, C. M., Otsuka, Y., Shiokawa, K., & Barros, D. (2018a). Medium scale traveling ionospheric disturbances observed by detrended total electron content maps over Brazil. *Journal of Geophysical Research: Space Physics*, *123*(3), 2215–2227. https://doi.org/10.1002/2017ja025021

Figueiredo, C. A. O. B., Takahashi, H., Wrasse, C. M., Otsuka, Y., Shiokawa, K., & Barros, D. (2018b). An investigation of nighttime MSTIDs observed by optical thermosphere imagers at low latitude: Morphology, propagation direction, and wind filtering. *Journal of Geophysical Research: Space Physics*, *123*, 7843–7857. https://doi.org/10.1029/2018JA025438

Figueiredo, C. A. O. B., Wrasse, C. M., Takahashi, H., Otsuka, Y., Shiokawa, K., & Barros, D. (2017). Large-scale traveling ionospheric disturbances observed by GPS dTEC maps over North and South America on Saint Patrick's Day storm in 2015. *Journal of Geophysical Research: Space Physics*, *122*(4), 4755–4763. https://doi.org/10.1002/2016JA023417

Forbes, J. M., Bruinsma, S. L., Doornbos, E., & Zhang, X. (2016). Gravity wave-induced variability of the middle thermosphere. *Journal of Geophysical Research: Space Physics*, *121*(7), 6914–6923. https://doi.org/10.1002/2016JA022923

Forbes, J. M., Bruinsma, S. L., Miyoshi, Y., & Fujiwara, H. (2008). A solar terminator wave in thermosphere neutral densities measured by the CHAMP satellite. *Geophysical Research Letters*, *35*(14), L14802. https://doi.org/10.1029/2008gl034075

Frissell, N. A., Baker, J. B. H., Ruohoniemi, J. M., Gerrard, A. J., Miller, E. S., Marini, J. P., et al. (2014). Climatology of medium-scale traveling ionospheric disturbances observed by the midlatitude Blackstone SuperDARN radar. *Journal of Geophysical Research: Space Physics*, *119*(9), 7679–7697. https://doi.org/10.1002/2014JA019870

Fritts, D. C., Lund, T. S., Wan, K., & Liu, H. L. (2021). Numerical simulation of mountain waves over the southern Andes. Part II: Momentum fluxes and wave–mean-flow interactions. *Journal of the Atmospheric Sciences*, *78*(10), 3069–3088. https://doi.org/10.1175/jas-d-20-0207.1

Fritts, D. C., & Vadas, S. L. (2008). Gravity wave penetration into the thermosphere: Sensitivity to solar cycle variations and mean winds. *Annales Geophysicae*, *26*(12), 3841–3861. https://doi.org/10.5194/angeo-26-3841-2008

Galvan, D. A., Komjathy, A., Hickey, M. P., Stephens, P., Snively, J., Song, Y. T., et al. (2012). Ionospheric signatures of Tohoku-Oki tsunami of March 11, 2011: Model comparisons near the epicenter. *Radio Science*, *47*(04), 1–10. https://doi.org/10.1029/2012rs005023

Gelaro, R., McCarty, W., Suárez, M. J., Todling, R., Molod, A., Takacs, L., et al. (2017). The Modern-Era Retrospective analysis for research and Applications, version 2 (MERRA-2). *Journal of Climate*, *30*(14), 5419–5454. https://doi.org/10.1175/JCLI-D-16-0758.1

Grocott, A., Hosokawa, K., Ishida, T., Lester, M., Milan, S. E., Freeman, M. P., et al. (2013). Characteristics of medium-scale traveling ionospheric disturbances observed near the Antarctic Peninsula by HF radar. *Journal of Geophysical Research: Space Physics*, *118*(9), 5830–5841. https://doi.org/10.1002/jgra.50515

Heale, C. J., Bossert, K., Vadas, S. L., Hoffmann, L., Dörnbrack, A., Stober, G., et al. (2020). Secondary gravity waves generated by breaking mountain waves over Europe. *Journal of Geophysical Research: Atmospheres*, *125*(5), e2019JD031662. https://doi.org/10.1029/2019jd031662

Heale, C. J., Snively, J. B., Bhatt, A. N., Hoffmann, L., Stephan, C. C., & Kendall, E. A. (2019). Multilayer observations and modeling of thunderstorm-generated gravity waves over the midwestern United States. *Geophysical Research Letters*, *46*(23), 14164–14174. https://doi.org/10.1029/2019gl085934

Hickey, M. P., Schubert, G., & Walterscheid, R. L. (2009). Propagation of tsunami-driven gravity waves into the thermosphere and ionosphere. *Journal of Geophysical Research*, *114*(A8). https://doi.org/10.1029/2009ja014105

Hines, C. O. (1960). Internal atmospheric gravity waves at ionospheric heights. *Canadian Journal of Physics*, *38*(11), 1441–1481. https://doi.org/10.1139/p60-150

Hocke, K., & Schlegel, K. (1996). A review of atmospheric gravity waves and travelling ionospheric disturbances: 1982–1995. In *Annales geophysicae* (Vol. 14, p. 917).

Hoffmann, L., Grimsdell, A. W., & Alexander, M. J. (2016). Stratospheric gravity waves at southern hemisphere orographic hotspots: 2003–2014 AIRS/Aqua observations. *Atmospheric Chemistry and Physics*, *16*(14), 9381–9397. https://doi.org/10.5194/acp-16-9381-2016

Hoffmann, L., Xue, X., & Alexander, M. J. (2013). A global view of stratospheric gravity wave hotspots located with Atmospheric Infrared Sounder observations. *Journal of Geophysical Research: Atmospheres*, *118*(2), 416–434. https://doi.org/10.1029/2012jd018658

Holton, J. R. (1992). *An introduction to dynamic meteorology* (3rd ed.). Academic Press.

Hunsucker, R. D., Zhao, J., Chu, X., & Becker, E. (1982). Atmospheric gravity waves generated in the high-latitude ionosphere: A review. *Reviews of Geophysics*, *20*, 293–315. https://doi.org/10.1029/2017JD027970

Ishida, T., Hosokawa, K., Shibata, T., Suzuki, S., Nishitani, N., & Ogawa, T. (2008). SuperDARN observations of daytime MSTIDs in the auroral and mid-latitudes: Possibility of long-distance propagation. *Geophysical Research Letters*, *35*(13), L13102. https://doi.org/10.1029/2008gl034623

Kotake, N., Otsuka, Y., Ogawa, T., Tsugawa, T., & Saito, A. (2007). Statistical study of medium-scale traveling ionospheric disturbances observed with the GPS networks in Southern California. *Earth Planets and Space*, *59*(2), 95–102. https://doi.org/10.1186/BF03352681

Kruse, C. G., Alexander, M. J., Hoffmann, L., van Niekerk, A., Polichtchouk, I., Bacmeister, J. T., et al. (2022). Observed and modeled mountain waves from the surface to the mesosphere near the Drake Passage. *Journal of the Atmospheric Sciences*, *79*(4), 909–932. https://doi.org/10.1175/jas-d-21-0252.1

Lane, T. P., Reeder, M. J., & Clark, T. L. (2001). Numerical modeling of gravity wave generation by deep tropical convection. *Journal of the Atmospheric Sciences*, *58*(10), 1249–1274. https://doi.org/10.1175/1520-0469(2001)058<1249:nmogwg>2.0.co;2

Liu, H., Pedatella, N., & Hocke, K. (2017). Medium-scale gravity wave activity in the bottomside F region in tropical regions. *Geophysical Research Letters*, *44*(14), 7099–7105. https://doi.org/10.1002/2017GL073855

Lund, T. S., Fritts, D. C., Wan, K., Laughman, B., & Liu, H. L. (2020). Numerical simulation of mountain waves over the southern Andes. Part I: Mountain wave and secondary wave character, evolutions, and breaking. *Journal of the Atmospheric Sciences*, *77*(12), 4337–4356. https://doi.org/10.1175/jas-d-19-0356.1

Makela, J. J., Lognonné, P., Hébert, H., Gehrels, T., Rolland, L., Allgeyer, S., et al. (2011). Imaging and modeling the ionospheric airglow response over Hawaii to the tsunami generated by the Tohoku earthquake of 11 March 2011. *Geophysical Research Letters*, *38*(24), L00G02. https://doi.org/10.1029/2011GL047860

Mannucci, A. J., Wilson, B. D., Yuan, D. N., Ho, C. H., Lindqwister, U. J., & Runge, T. F. (1998). A global mapping technique for GPS-derived ionospheric total electron content measurements. *Radio Science*, *33*(3), 565–582. https://doi.org/10.1029/97rs02707

Marengo, J. A. (2004). Interdecadal variability and trends of rainfall across the Amazon basin. *Theoretical and Applied Climatology*, *78*(1–3), 79–96. https://doi.org/10.1007/s00704-004-0045-8

Martinis, C., Baumgardner, J., Smith, S. M., Colerico, M., & Mendillo, M. (2006). Imaging science at El Leoncito, Argentina. *Annales Geophysicae*, *24*(5), 1375–1385. https://doi.org/10.5194/angeo-24-1375-2006

Martinis, C., Yokoyama, T., & Nishioka, M. (2019). All-sky imaging observations and modeling of Bright 630-nm airglow structures associated with MSTIDs. *Journal of Geophysical Research: Space Physics*, *124*(8), 7332–7340. https://doi.org/10.1029/2019JA026935

Miyoshi, Y., Jin, H., Fujiwara, H., & Shinagawa, H. (2018). Numerical study of traveling ionospheric disturbances generated by an upward propagating gravity wave. *Journal of Geophysical Research: Space Physics*, *123*(3), 2141–2155. https://doi.org/10.1002/2017JA025110

Munro, G. H. (1948). Short-period changes in the F region of the ionosphere. *Nature*, *162*(4127), 886–887. https://doi.org/10.1038/162886a0

Negale, M. R., Taylor, M. J., Nicolls, M. J., Vadas, S. L., Nielsen, K., & Heinselman, C. J. (2018). Seasonal propagation characteristics of MSTIDs observed at high latitudes over central Alaska using the Poker Flat incoherent scatter radar. *Journal of Geophysical Research: Space Physics*, *123*(7), 5717–5737. https://doi.org/10.1029/2017JA024876

Neuhäuser, M. (2011). Wilcoxon–Mann–Whitney test. In M. Lovric (Ed.), *International encyclopedia of statistical science*. Springer. https://doi.org/10.1007/978-3-642-04898-2_615

Nicolls, M. J., Vadas, S. L., Aponte, N., & Sulzer, M. P. (2014). Horizontal parameters of daytime thermospheric gravity waves and E region neutral winds over Puerto Rico. *Journal of Geophysical Research: Space Physics*, *119*(1), 575–600. https://doi.org/10.1002/2013JA018988

Nicolls, M. J., Varney, R. H., Vadas, S. L., Stamus, P. A., Heinselman, C. J., Cosgrove, R. B., & Kelley, M. C. (2010). Influence of an inertia-gravity wave on mesospheric dynamics: A case study with the Poker Flat Incoherent Scatter Radar. *Journal of Geophysical Research*, *115*, D00N02. https://doi.org/10.1029/2010JD014042

Nishioka, M., Tsugawa, T., Kubota, M., & Ishii, M. (2013). Concentric waves and short-period oscillations observed in the ionosphere after the 2013 Moore EF5 tornado. *Geophysical Research Letters*, *40*(21), 5581–5586. https://doi.org/10.1002/2013GL057963

Occhipinti, G., Lognonné, P., Kherani, E. A., & Hébert, H. (2006). Three-dimensional waveform modeling of ionospheric signature induced by the 2004 Sumatra tsunami. *Geophysical Research Letters*, *33*(20), L20104. https://doi.org/10.1029/2006gl026865

Oncken, O., Chong, G., Franz, G., Giese, P., Götze, H. –J., Ramos, V., et al. (2006). *The Andes*. Springer.

Otsuka, Y. (2021). Medium-scale traveling ionospheric disturbances. In C. Huang, G. Lu, Y. Zhang, & L. J. Paxton (Eds.), *Ionosphere dynamics and applications*. https://doi.org/10.1002/9781119815617.ch18

Otsuka, Y., Kotake, N., Shiokawa, K., Ogawa, T., Tsugawa, T., & Saito, A. (2011). Aeronomy of the Earth's atmosphere and ionosphere. In *Statistical study of medium-scale traveling ionospheric disturbances observed with a GPS receiver network in Japan* (pp. 291–299). Springer.

Otsuka, Y., Suzuki, K., Nakagawa, S., Nishioka, M., Shiokawa, K., & Tsugawa, T. (2013). GNSS observations of medium-scale traveling ionospheric disturbances over Europe. *Annales Geophysicae*, *31*(2), 163–172. https://doi.org/10.5194/angeo-31-163-2013

Park, J., Lühr, H., Lee, C., Kim, Y. H., Jee, G., & Kim, J.-H. (2014). A climatology of medium-scale gravity wave activity in the midlatitude/low-latitude daytime upper thermosphere as observed by CHAMP. *Journal of Geophysical Research: Space Physics*, *119*(3), 2187–2196. https://doi.org/10.1002/jgra.50886

Paulino, I., Medeiros, A. F., Vadas, S. L., Wrasse, C. M., Takahashi, H., Buriti, R. A., et al. (2016). Periodic waves in the lower thermosphere observed by OI 630 nm airglow images. *Annales Geophysicae*, *34*(2), 293–301. https://doi.org/10.5194/angeo-34-293-2016

Roble, R. G., & Ridley, E. C. (1994). A thermosphere-ionosphere-mesosphere-electrodynamics general circulation model (time-GCM): Equinox solar cycle minimum simulations (30–500 km). *Journal of Geophysical Research*, *21*(6), 417–420. https://doi.org/10.1029/93GL03391

Sato, K., Tanteno, S., Watanabe, S., & Kawatani, Y. (2012). Gravity wave characteristics in the Southern hemisphere revealed by a high-resolution middle-atmosphere general circulation model. *Journal of the Atmospheric Sciences*, *69*(4), 1378–1396. https://doi.org/10.1175/JAS-D-11-0101.1

Sherstyukov, R. O., Akchurin, A. D., & Sherstyukov, O. N. (2018). Collocated ionosonde and dense GPS/GLONASS network measurements of midlatitude MSTIDs. *Advances in Space Research*, *61*(7), 1717–1725. ISSN 0273-1177. https://doi.org/10.1016/j.asr.2017.11.026

Shiokawa, K., Ihara, C., Otsuka, Y., & Ogawa, T. (2003). Statistical study of nighttime medium-scale traveling ionospheric disturbances using midlatitude airglow images. *Journal of Geophysical Research*, *108*(A1), 1052. https://doi.org/10.1029/2002JA009491

Sivakandan, M., Otsuka, Y., Ghosh, P., Shinagawa, H., Shinbori, A., & Miyoshi, Y. (2021). Comparison of seasonal and longitudinal variation of daytime MSTID activity using GPS observation and GAIA simulations. *Earth Planets and Space*, *73*(1), 35. https://doi.org/10.1186/s40623-021-01369-5

Smith, S. M., Vadas, S. L., Baggaley, W. J., Hernandez, G., & Baumgardner, J. (2013). Gravity wave coupling between the mesosphere and thermosphere over New Zealand. *Journal of Geophysical Research: Space Physics*, *118*(5), 2694–2707. https://doi.org/10.1002/jgra.50263

Takahashi, H., Essien, P., Figueiredo, C. A. O. B., Wrasse, C. M., Barros, D., Abdu, M. A., et al. (2021). Multi-instrument study of longitudinal wave structures for plasma bubble seeding in the equatorial ionosphere. *Earth and Planetary Physics*, *5*(5), eepp2021047. https://doi.org/10.26464/epp2021047

Takahashi, H., Wrasse, C. M., Figueiredo, C. A. O. B., Barros, D., Abdu, M. A., Otsuka, Y., & Shiokawa, K. (2018). Equatorial plasma bubble seeding by MSTIDs in the ionosphere. *Progress in Earth and Planetary Science*, *5*(1), 32. https://doi.org/10.1186/s40645-018-0189-2

Takahashi, H., Wrasse, C. M., Figueiredo, C. A. O. B., Barros, D., Paulino, I., Essien, P., et al. (2020). Equatorial plasma bubble occurrence under propagation of MSTID and MLT gravity waves. *Journal of Geophysical Research: Space Physics*, *125*(9), e2019JA027566. https://doi.org/10.1029/2019JA027566

Terra, P., Vargas, F., Brum, C. G. M., & Miller, E. S. (2020). Geomagnetic and solar dependency of MSTIDs occurrence rate: A climatology based on airglow observations from the Arecibo observatory ROF. *Journal of Geophysical Research: Space Physics*, *125*(7), e2019JA027770. https://doi.org/10.1029/2019JA027770

Torrence, C., & Compo, G. P. (1998). A practical guide to wavelet analysis. *Bulletin of the American Meteorological Society*, *79*(1), 61–78. https://doi.org/10.1175/1520-0477(1998)079<0061:APGTWA>2.0.CO;2

Trinh, Q. T., Ern, M., Doornbos, E., Preusse, P., & Riese, M. (2018). Satellite observations of middle atmosphere–thermosphere vertical coupling by gravity waves. *Annales Geophysicae*, *36*(2), 425–444. https://doi.org/10.5194/angeo-36-425-2018

Tsugawa, T., Kotake, N., Otsuka, Y., & Saito, A. (2007). Medium-scale traveling ionospheric disturbances observed by GPS receiver network in Japan: A short review. *GPS Solutions*, *11*(2), 139–144. https://doi.org/10.1007/s10291-006-0045-5

Vadas, S. L. (2007). Horizontal and vertical propagation and dissipation of gravity waves in the thermosphere from lower atmospheric and thermospheric sources. *Journal of Geophysical Research*, *112*(A6), A06305. https://doi.org/10.1029/2006JA011845

Vadas, S. L., & Azeem, I. (2020). Concentric secondary gravity waves in the thermosphere over the continental US on 25–26 March 2015 from deep convection. *Journal of Geophysical Research: Space Physics*, *126*(2). https://doi.org/10.1029/2020JA028275

Vadas, S. L., & Becker, E. (2019). Numerical modeling of the generation of tertiary gravity waves in the mesosphere and thermosphere during strong mountain wave events over the Southern Andes. *Journal of Geophysical Research: Space Physics*, *124*(9), 7687–7718. https://doi.org/10.1029/2019JA026694

Vadas, S. L., & Crowley, G. (2010). Sources of the traveling ionospheric disturbances observed by the ionospheric TIDDBIT sounder near Wallops Island on 30 October 2007. *Journal of Geophysical Research*, *115*(A7), A07324. https://doi.org/10.1029/2009JA015053

Vadas, S. L., Liu, H.-L., & Lieberman, R. S. (2014). Numerical modeling of the global changes to the thermosphere and ionosphere from the dissipation of gravity waves from deep convection. *Journal of Geophysical Research: Space Physics*, *119*(9), 7762–7793. https://doi.org/10.1002/2014JA020280

Vadas, S. L., Makela, J. J., Nicolls, M. J., & Milliff, R. F. (2015). Excitation of gravity waves by ocean surface wave packets: Upward propagation and reconstruction of the thermospheric gravity wave field. *Journal of Geophysical Research: Space Physics*, *120*(11), 9748–9780. https://doi.org/10.1002/2015JA021430

Vadas, S. L., & Nicolls, M. J. (2009). Temporal evolution of neutral, thermospheric winds and plasma response using PFISR measurements of gravity waves. *Journal of Atmospheric and Solar-Terrestrial Physics*, *71*(6–7), 744–770. https://doi.org/10.1016/j.jastp.2009.01.011

Vadas, S. L., Suzuki, H., Nicolls, M. J., Nakamura, T., & Harmon, R. O. (2014). Atmospheric gravity waves excited by a fireball meteor: Observations and modeling. *Journal of Geophysical Research: Space Physics*, *119*(14), 8583–8605. https://doi.org/10.1002/2014JD021664

Vadas, S. L., Xu, S., Yue, J., Bossert, K., Becker, E., & Baumgarten, G. (2019). Characteristics of the quiet-time hot spot gravity waves observed by GOCE over the Southern Andes on 5 July 2010. *Journal of Geophysical Research: Space Physics*, *124*(8), 7034–7061. https://doi.org/10.1029/2019JA026693

Vadas, S. L., Zhao, J., Chu, X., & Becker, E. (2018). The excitation of secondary gravity waves from local body forces: Theory and observation.

Xu, S., Vadas, S. L., & Yue, J. (2021). Thermospheric traveling atmospheric disturbances in austral winter from GOCE and CHAMP. *Journal of Geophysical Research: Space Physics*, *126*(9), e2021JA029335. https://doi.org/10.1029/2021ja029335

Xu, S., Yue, J., Xue, X., Vadas, S. L., Miller, S. D., Azeem, I., et al. (2019). Dynamical coupling between hurricane Matthew and the middle to upper atmosphere via gravity waves. *Journal of Geophysical Research: Space Physics*, *124*(5), 3589–3608. https://doi.org/10.1029/2018ja026453

Zabotin, N. A., Godin, O. A., & Bullett, T. W. (2016). Oceans are a major source of waves in the thermosphere. *Journal of Geophysical Research: Space Physics*, *121*(4), 3452–3463. https://doi.org/10.1002/2016ja022357